Chapter 4 Satellite image analysis

4-1 Data processing of the LANDSAT TM image

4-1-1 Satellite data and processing

In this survey, image analysis was carried out with the ASTER data. Images used for regions whose ASTER image was not obtained were covered by mosaic images of ten scenes of LANDSAT 5 TM, which were prepared in the regional survey for mineral resource carried out as part of the 1997 basic survey for cooperation in resource development in the Argentine Republic. The index images is shown in Fig. II-4-1-1-1, and dates of observation of each image and information on the position of the sun are as shown in Table II-4-1-1.

False color mosaic images prepared with a combination of BGR=145 suitable for mapping geological structure in andesitic volcanic rocks and resampled by the geometric conversion method by which 16 pixels (4 x 4) are made to be one pixel with bi-linear interpolation.

The projection method used for images is as follows.

Projection: Transverse Mercator (UTM)

Spheroid: International 1909

Central Meridian: -69

False easting 500000

False northing 10000000

Table II-4-1-1 Path/Row, data acquisiton, sun azimuth and sun elevation of the Landsat TM image

Area	Image name	Path	Row	Date	Sun azimuth	Sun elevation
Tupiza	Tupiza	232	75	1990/ 4/22/	N53°E	38°
Susques	Susques	232	76	1991/ 2/ 4/	N89°E	48°
Pocitos	Salar de Pocitos	232	77	1991/ 2/ 4/	N87°E	48°
Antofagasta	Antofagasta de la Sierra	232	78	1987/ 2/ 9/	N84°E	47°
Belen	Belen	232	79	1987/ 2/ 9/	N82°E	47°
Tarija	Tarija	231	75	1986/ 9/11/	N59°E	44°
San Ramon	San Ramon de la Nueva Oran	231	76	1986/ 9/11/	N58°E	43°
Salta	Salta	231	77	1986/ 9/11/	N57°E	42°
Rosario	Rosario de Frontera	231	78	1986/ 9/11/	N57°E	41°
Tucuman	San Miguel de Tucuman	231	79	1986/ 9/11/	N57°E	40°

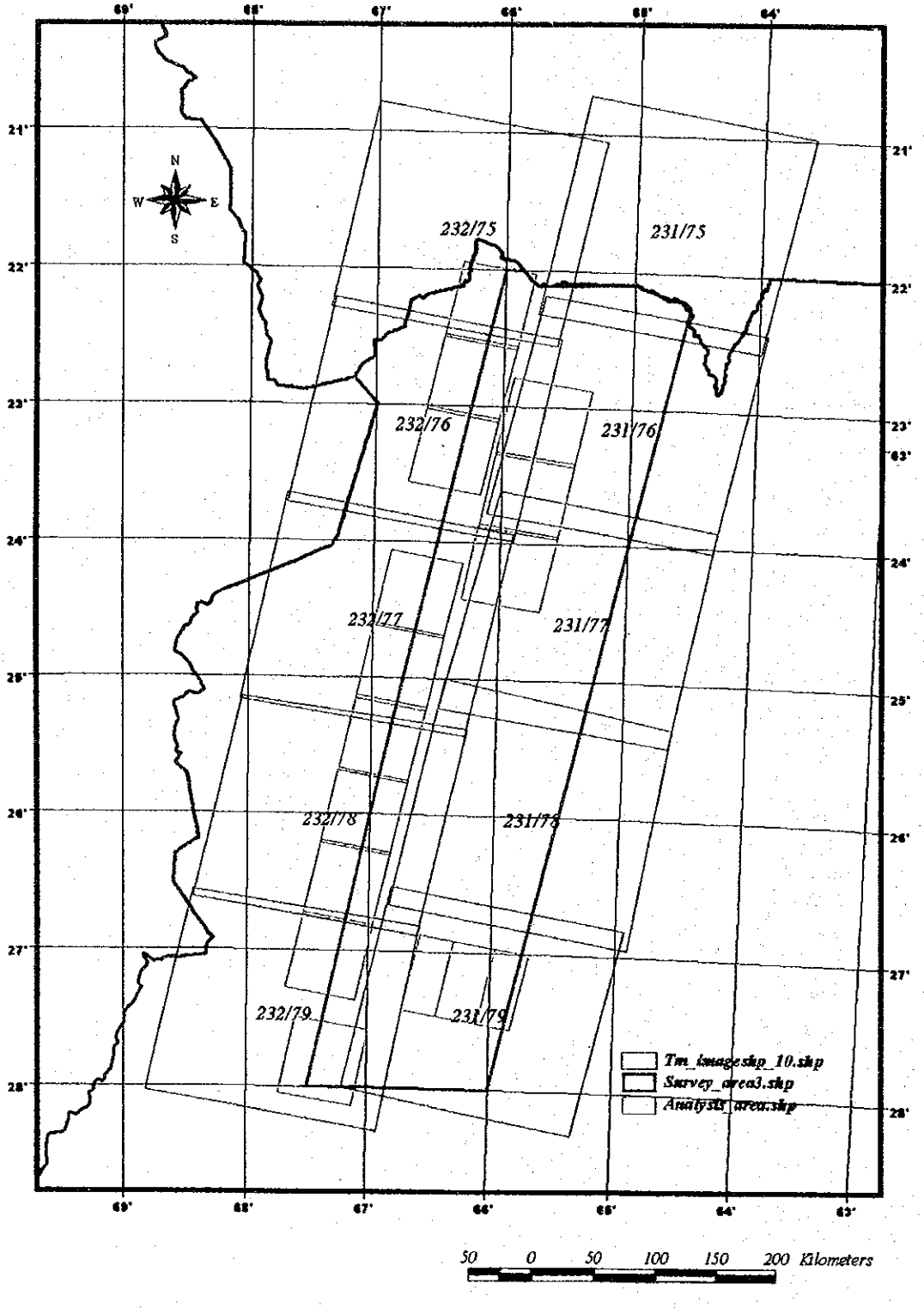

Fig.II-4-1-1-1 Image analysis area of Landsat TM

4-2 Analysis and interpretation of LANDSAT TM images

To contribute to selection of potential areas, the vast area spreading from the south end portion of the Republic of Bolivia to Mendoza, the Argentine Republic, was covered by the analysis carried out as part of the regional survey for mineral resources in 1997. In the survey, geology and mineral deposits and mineral showings were checked by photo-geological interpretation through the use of LANDSAT TM images and other existing data. The survey area was covered by 23 scenes of LANDSAT TM images and false color image, band ratioing composites and a false color digital mosaic image were processed, then geology and geological structure were interpreted and alteration zones were outlined. Finally, by comprehensively interpreting them, high potential are for mineral deposits were selected.

The survey area of 2001 year is included in ten scenes on the northeastern part among these 23 scenes of the 1997 survey. Mosaic images, alteration zones and lineaments from results of the analysis in 1997 were was used for 2001 interpretation.

4-3 Data processing of the ASTER image

4-3-1 Outline of analysis

The purpose of this analysis covering arid areas is to identify alteration minerals with the ASTER, which was designed for effective mineral exploration. Prior to the analysis, image quality evaluation and bands registration were executed. Images were exactly consistent with one another among VNIR bands, but some address errors of pixels in images were confirmed among bands of SWIR and among of VNIR and SWIR. Therefore, images was corrected by the least square method with a two-dimensional quadric polynomial expression used after calculation of matching vectors by template matching using the area correlation method. After correcting registration errors, pseudo reflectance conversion was applied for 15 scenes. The conversion were calculated based on characteristics of spectral reflectance of Pampa distributed in the survey area, because the fact that the ratio between bands of surface materials of Pampa is almost constant regardless of areas, and this is the first trial to use this method for practical filed survey. Pseudo reflectance conversion coefficient were based on METI(2001). Minerals identification is the main object of this analysis, and characteristics of spectral reflectance are used for this identification. Therefore, it can be said that accuracy of pseudo reflectance conversion is an important correction that determines the accuracy of analysis.

The survey area is nearly non-vegetated, but sparse vegetation is recognized in the mountainous zone on the east side of the survey area. In zones where vegetation grow sparsely on soils, reflectance spectra are affected by the reflectance spectra of plants. If minerals are identified by reflectance spectra mixed with vegetation, a large amount of alunite and kaolinite will be detected. A spectral reflectance mixed with vegetation can be represented by a composite sum

corresponding to the area ratio between reflectance spectra of bare rock/soil and the reflectance spectra of plants. Reflectance spectra of plants were removed by the use of the SAVI (Soil Adjust Vegetation Index) for this area ratio, and by the use of the fact that a SAVI value functions as an index of vegetation cover ratio. Then, almost satisfactory results could be obtained for areas with the percentage of vegetation cover of up to 50%.

For identification and semi-quantitative analysis of alteration minerals, a iso-grain model is used. The weathered ground surface generally consists of a mixture of several or more kinds of minerals. Therefore, with the iso-grain model, for which reflection and absorption among mineral grains are taken into consideration, it is possible to explain changes of reflectance spectra of this mixture theoretically. In this analysis, nine minerals widely observed were selected, and a database of spectral reflection with a mixture of these minerals was created with the iso-grain model. Next, comparing image data and spectral reflectance per one pixel, minerals are identified and mapped.

SiO_2 content mapping was carried out using the conversion method proposed in METI(2000)., after radiometric correction(remove atmospheric effects) and temperature-emissivity separation were applied for thermal bands data that are characteristic of the ASTER.

***ASTER**

The ASTER (Advanced Space-borne Thermal Emission and Reflection Radiometer) is a multiple-band high-discrimination sensor developed by the Ministry of Economy, Trade and Industry (METI). It was launched on board the first earth resource satellite, "Terra", in an ongoing international cooperation project named the EOS Program under the leadership of the Aeronautics and Space Administration (NASA) on December 1999.

The ASTER was developed to succeed the conventional JERS-1-equipped with optical sensor, OPS. It has two additional bands for the short wavelength infrared range (SWIR) and five additional bands for the thermal infrared range (TIR) in comparison with OPS. This has enabled detailed classification of hydrothermal alteration zones and silicate rocks, which had been impossible, and also has allowed silicate content in rock to be estimated by the spectrum absorption of silicate in the thermal infrared range. Particularly, TIR is the first full-scale thermal infrared sensor on board an artificial satellite, and it attracts attention as a device that contributes to identification of rocks.

4-3-2 Data used

The fifteen scenes used are shown below. Data was retrieved by the image retrieval system (ASTER GDS) of the Resource and Environment Observation and Analysis Center(ERSDAC). The best images with lesser amounts of clouds at that time (August 2001) were selected, and given by ERSDAC.

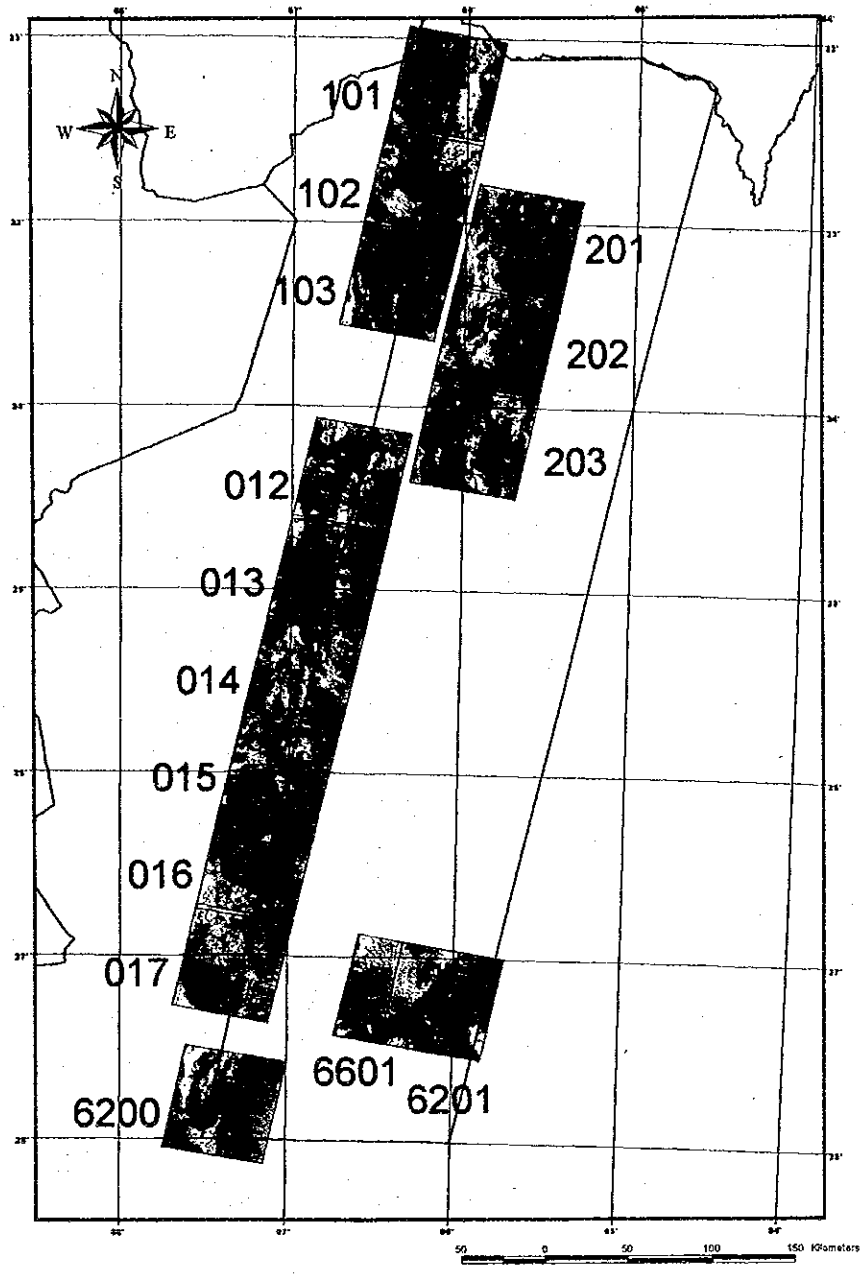

Fig.II-4-3-2-1 Index map of ASTER image over the survey area

Table II-4-3-1 Acquisition data of ASTER image

scene id	granule id	lat.center	lon.center	acq. date	condition
12	ASTL1B0009091451200010125801	-24.24'	-66.37'	2000/9/9	fair(some snow)
13	ASTL1B0009091451290010125787	-24.56'	-66.45'	2000/9/9	fair(some snow)
14	ASTL1B0009091451380010125788	-25.28'	-66.53'	2000/9/9	fair
15	ASTL1B0009091451470010125789	-26.00'	-67.02'	2000/9/9	fair
16	ASTL1B0009091451560010125790	-26.32'	-67.10'	2000/9/9	fair
17	ASTL1B0009091452040010125791	-27.04'	-67.18'	2000/9/9	fair
101	ASTL1B0009091450450010125800	-22.16'	-66.06'	2000/9/9	partly clouds
102	ASTL1B0009091450450010125802	-22.48'	-66.13'	2000/9/9	partly clouds
103	ASTL1B0101061455470101190033	-27.50'	-67.21'	2000/9/9	partly clouds
201	ASTL1A0008311457080012281005	-23.07'	-65.41'	2000/8/31	fog, clouds
202	ASTL1A0008311457160012281006	-23.39'	-65.48'	2000/8/31	fog, clouds
203	ASTL1A0008311457250012281007	-24.11'	-65.56'	2000/8/31	fog, clouds
6200	ASTL1B0101061455470101190033	-27.50'	-67.21'	2001/1/6	partly clouds
6201	ASTL1B0101311449070102230750	-27.15'	-66.04'	2001/1/31	partly clouds
6601	ASTL1B0103201447450103301315	-27.12'	-66.20'	2001/3/20	partly clouds
6602	ASTL1B0103201447540103301364	-27.44'	-66.28'	2001/3/20	for radiance correction

Data 012 to 017 are good images, although snow is partly covered. Data 101 to 103 were taken on the same day as Data 012 to 017. Bluish stripe-like clouds are partly observed, and there are regions of shadows corresponding to clouds. These were taken in September, which falls in winter in this district. The sun elevation is about 45 degrees, which is relatively low, and southwest slopes out of the sun between mountains are very dark. On Data 201 to 203, bluish stripe-like clouds are partly recognized, and there are corresponding shadows. As the sun elevation was low, since these were taken at the end of August, southwest slopes are very dark. Therefore, analyses are impossible in most of these three zones. Data 6200 is located on the south side of Data 017, and it was taken in January. As the sun elevation was high, since it was summer in this district, these were taken in the period good for analysis. Clouds in a band shape were recognized in the northwest part on the image, and vegetations are observed between mountains. Data 6201 is located to the northeast of Data 6200. Clouds in a band shape are partly recognized, and many places between mountains are thickly covered with vegetation. Data 6601 is located on the west side of Data 6201, and about half of the region overlaps with Data 6201. Although about half of Data 6201 is covered with clouds, because this data overlaps with Data 6201 as mentioned above, either can be used. In this area, places between mountains are also thickly covered with plants. Data 6601 is widely covered with clouds and vegetation, and sufficient statistic quantity for pseudo reflectance conversion cannot be calculated. Therefore, Data 6602 was used as reference data for the calculation of statistic values.

4-3-3 Band registration

Spatial resolution of Band 1 to 3 is 15 m (4980 x 4200 pixels), while that of Band 4 to 9 is 30 m (2490 x 2100 pixels). Therefore, images of Band 1 to 3 were scaled down by half to make them of the same size as those in the SWIR. For the reduction scale, the method by which 2 x 2 pixel were given as the average value was used. Therefore, the volume of data is 2490 x 2100 x 9 bands ≒ 45 M bytes.

In the ASTER 1 B data, some pixel location error is recognized among bands. In particular, the location error was large between the VNIR/SWIR and the SWIR, and identification of minerals could not be carried out as they were, so band registration was needed. Band 2 is selected as registration standard, and Bands 1, 3 and 4 were made to be consistent with images of Band 2. For Band 5, matching was carried out with Band 4 deformed by registration as a basis. For all bands following Band 5, registration was carried out with the band deformed by the previous registration as a basis.

For the registration, a template of 401 x 401 was used, and the image correlation method to calculate correlation coefficients of radiance between images at all points inside the template was also used. The searching area was set to be a range of 12 pixels from the initial point to the upper, lower, right and left sides, respectively (25 x 25 in total, 625 repetitions). Then the image correlation method was employed and image correlation coefficients are calculated at all points(625) in the template every time one point is shifted. From these, the position where an image correlation coefficient is the largest was taken as a matching position.

A matching vector of every 500 points was calculated at five points in the direction of right and left and at four points in the direction of top and bottom: 20 points in total. With this as a two-dimensional quadric polynomial expression, geometrical conversion coefficients were calculated by the least square method and the most adjacent interpolation was used for deformation. The geometrical conversion expression is as follows:

$$u=a_1x^2+b_1xy+c_1y^2+d_1x+e_1y+g_1$$

$$v=a_2x^2+b_2xy+c_2y^2+d_2x+e_2y+g_2$$

where a_1 to g_2 are coefficients, x and y are positions of image before deformation, and u and v are moving vectors.

After geometrical conversion, matching vectors were calculated again in the same way, and the results of deformation were checked. Table II-4-3-2 shows matching vectors before deformation, and Table II-4-3-3 shows those after deformation. As shown in the tables, registration among bands was accurately done.

Table II-4-3-2 Data012 Pixel location error between band4 and band5(before registration)

		X-direction				
		250	750	1250	1750	2250
Y - direct.	250	-2,-2 *0.9468*	-2,-3 *0.9805*	-2,-2 *0.9498*	-1,-2 *0.9529*	-1,-2 *0.9479*
	750	-2,-2 *0.9310*	-2,-2 *0.8838*	-2,-20.9582	-1,-3 *0.9817*	-1,-2 *0.8998*
	1250	-2,-3 *0.9369*	-2,-2 *0.9646*	-1,-2 *0.9584*	-1,-2 *0.9311*	+3,-1 *0.8264*
	1750	-2,-2 *0.9686*	-2,-2 *0.9368*	-1,-1 *0.8819*	-1,-1 *0.9432*	————

The first value in each column shows Y-direction, the second is sift of Y-direction, the third is image correlation coefficient.

Table II-4-3-3 Data012 Pixel location error between band4 and band5(after registration)

		X-direction				
		250	750	1250	1750	2250
Y - direct.	250	0,0 *0.9468*	0,1 *0.9805*	0,0 *0.9498*	0,0 *0.9529*	0,0 *0.9479*
	750	0,0 *0.9310*	0,0 *0.8838*	0,00.9582	0,1 *0.9817*	0,0 *0.8998*
	1250	0,0 *0.9369*	0,0 *0.9646*	0,0 *0.9584*	0,0 *0.9311*	-3,1 *0.8264*
	1750	0,0 *0.9686*	0,0 *0.9368*	0,1 *0.8819*	1,1 *0.9432*	————

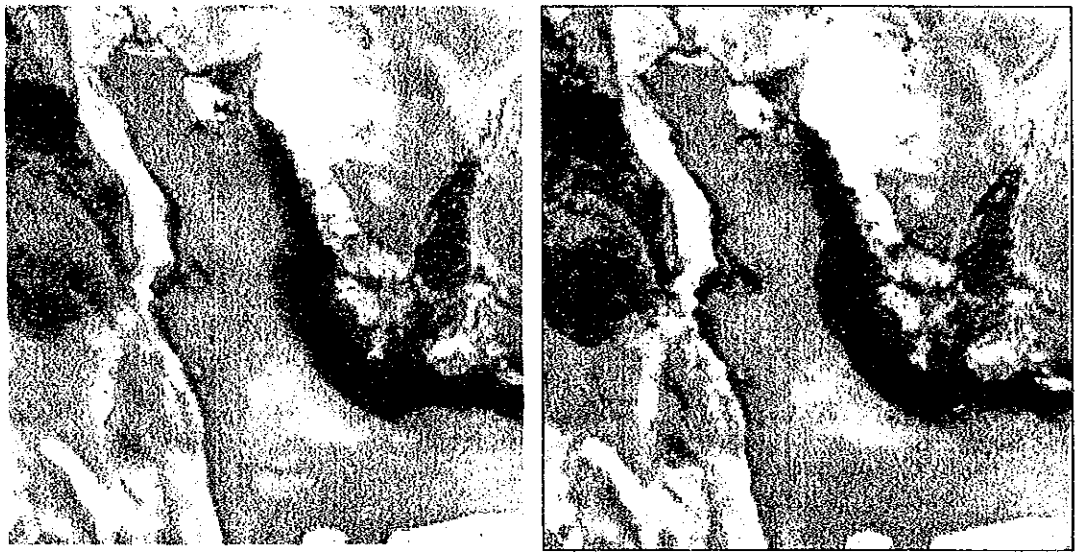

(a) (b)

Fig.II-4-3-3-1 A processing step for band to band registration

4-3-4 Pseudo reflectance conversion

Radiance value in ASTER data is a digital number of 256 gradations of digital values quantified by applying gain and bias independently per band. This value expresses an intensity ratio of relative reflectance in a band, but comparison of the values is nonsense. Therefore, if identification of minerals is carried out in the patterns of Bands 1 to 9, it is necessary to convert radiance values among bands to comparable numeric values by some manner. This is pseudo reflectance conversion and with this conversion, minerals can be identified from absorption patterns of the band.

The log residuals method is one of the pseudo reflectance correction method which has been proposed so far. In this method, a statistic of images is used and it is said that log residuals values represent good approximate values of pseudo reflectance on the following assumptions:

* An average value of the radiance value of each band is constant on the whole image (pseudo reflectance is horizontal).
* Standard deviation of the radiance value of each band is constant on the whole image.

Surface materials meeting these conditions, however, have not been clarified, and verification of this hypothesis requires measurement of spectral reflectance in a vast area, which is impossible. Therefore, it is reasonable to consider that the log residuals method is an ambiguous pseudo reflectance conversion method that cannot be examined for the hypothesis conditions. In fact, the METI(1997) showed that pseudo reflectance obtained from a log residuals value in arid regions was greatly different from that actually measured in the field verification.

A conversion coefficient of pseudo reflectance conversion is not fixed at a certain numeric value for each satellite. This is because atmospheric transmittance varies from day to day according to conditions of the air. The influence of air is larger in the VNIR, and transmittance fluctuates largely according to conditions of the air in regions with a shorter wavelength. This is more easily understood by considering the phenomena that mountains in the distance cannot been seen or look blue and dim.

METI(2000) carried out pseudo reflectance conversion by measuring indoors reflectance of gravel of Pampa sampled on the site, and then fitting to this reflectance. This is a pseudo reflectance conversion method that does not require atmospheric correction. The greatest disadvantage is, however, that a sample is required. In areas without any samples, like this case, this method cannot be used. For this reason, we developed a method of conversion into pseudo reflectance for this analysis, using optical properties of the surface materials of Pampa. This method is as follows:

① Identification of materials without characteristic reflectance spectra, mainly at Pampa.
② Calculation of intensity ratios between bands of extracted materials
③ Identification of materials without characteristic spectral reflectance in areas with known pseudo reflectance (mainly at Pampa)

④ Calculation of the intensity ratio among bands of materials extracted in ③.

⑤ Calculation of a conversion coefficient to make consistent the intensity ratios obtained in ② and ④.

By the operation mentioned above, radiance ratios between bands in the analysis area can be corrected to be radiance ratios between bands in the areas where the pseudo reflectance conversion coefficient has already been found. As the coefficient is known in the area of ③, data of the analysis area can be converted to pseudo reflectance by multiplying by this value.

As this method requires data with known pseudo reflectance conversion coefficients, the results of analysis by the METI(2001) were used. Accordingly, if the pseudo reflectance conversion coefficients in this data are wrong, this analysis is also wrong. But because these results are good, it is considered that our correction coefficient is right on the whole.

(1) Bands characteristics in the whole image area

In data successively obtained on the same day in a arid region, conditions of the air are considered to be almost constant. Scatter diagrams of ratios between bands are prepared per scene, and a very interesting fact is found.

Fig. II-4-3-4-1 shows a comparison, among scenes, of the scatter diagrams of Bands 2 and 3 of Data 012 to 017. These diagrams were prepared from the whole image area. On the scatter diagrams, parts where the frequency of data appearance is high are expressed with warm colors, and those with low frequency are expressed with cold colors. With this coloring, it is found that a scatter diagram without vegetation is plotted in a shape with slope in a very narrow region. This indicates that the lightness of rock varies but color tones are almost similar. In fact, it is known from field surveys that bare rock areas show a similar liver brown color. What is important is that, although the kinds of dominant rock are different according to the scenes, the directions of extension of regions with data concentration recognized on the scatter diagrams do not differ among scenes.

On images of the same area obtained on different days, the above-mentioned slope is generally not consistent. This is because transmittance per wavelength changes according to conditions of the air. However, if the fact that, even if the kinds of distributed rock are different, the slope of the ratio between bands is almost constant is held in any band, conversion into data that has a fixed relation between bands is possible even in a different scene by correcting the ratio between the bands to be a certain value.

Fig. II-4-3-4-2 shows scatter diagrams between bands of Data 102. These diagrams show that a scatter diagram between adjacent bands in the SWIR has more concentration of data than the band 2/3 ratio, and that almost all rocks have similar characteristics of reflectance spectra in the SWIR. Even though scenes are different, the direction of the largest extension of the region with concentration on the scatter diagram does not change practically.

Band 3/4 is poor in concentration on the scatter diagram, and there are some cases where such specific tendency that the ratio between bands is constant cannot be found on the scatter diagram prepared for the whole region.

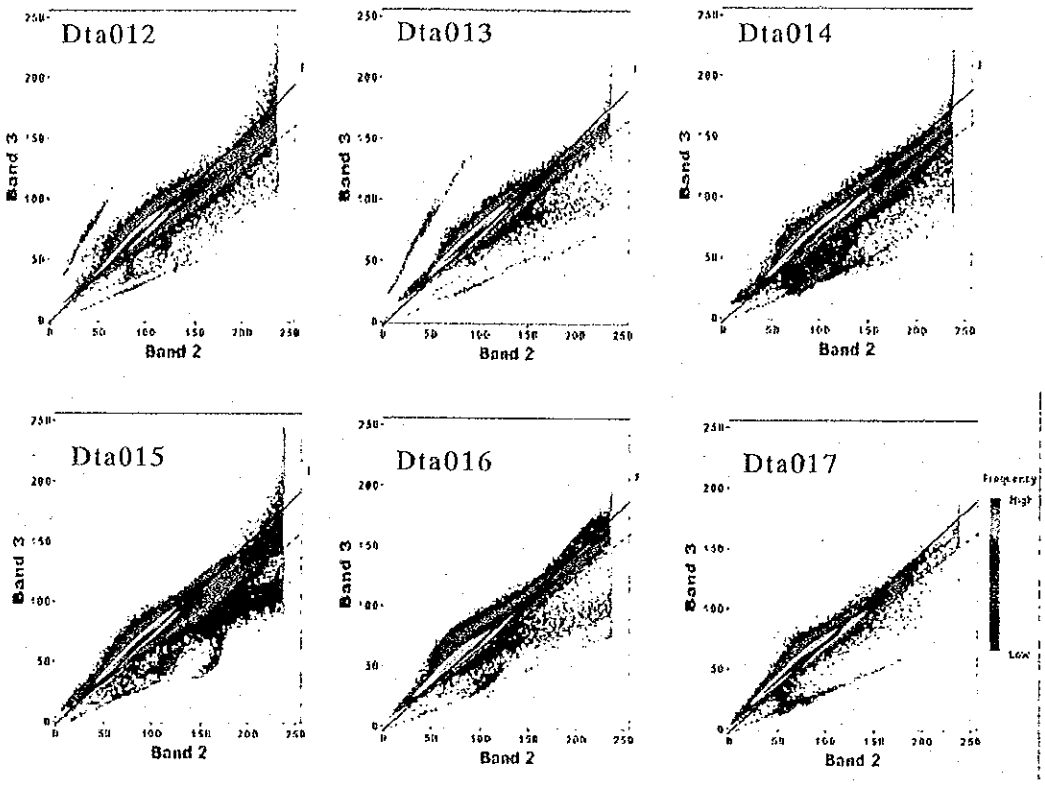

Fig.II-4-3-4-1 Scatter diagrams of DN between Data012～017

Graphs are scatter diagrams of the radiance value(DN) of Band 2/3 in six scenes of Data 012 to 017. Colors on the scatter diagrams express the density of data, and warm colors represent regions where data is distributed densely.

The black solid line in this figure shows that the slope obtained from the direction of the largest extension of radiance value distribution in the scatter diagram of Data 012 is shown on scatter diagrams of other scenes. As known from the graphs, even if surface materials (geological units) differ among images obtained on the same day, the shape of distribution of scatter diagrams does not differ practically.

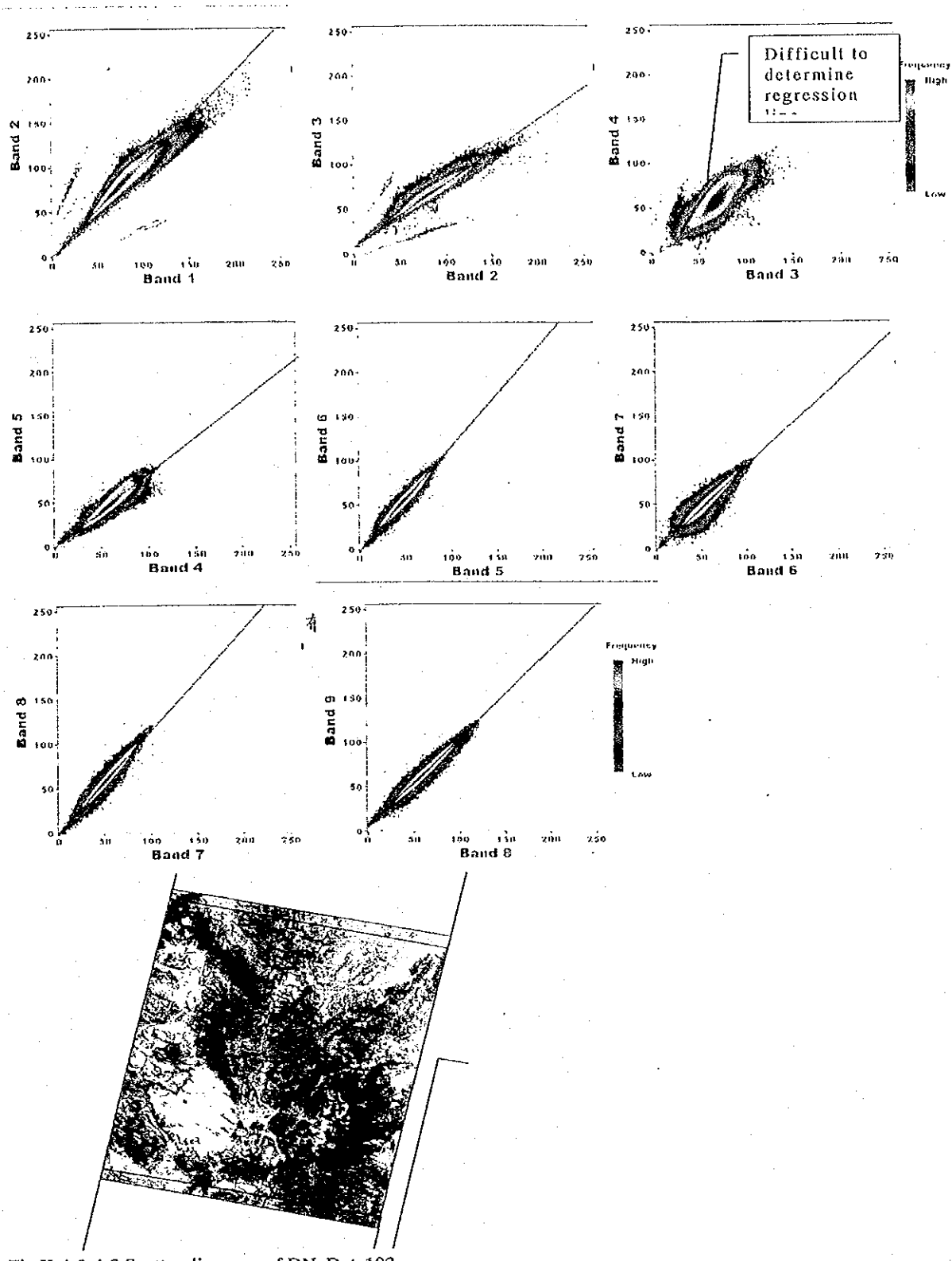

Fig.II-4-3-4-2 Scatter diagrams of DN, Data102

(In Band 3/4, the scatter diagram has bad concentration, and such relation that the ratio is constant cannot be found.)

(2) Bands characteristics in the high correlation area

Among adjacent bands in the SWIR, correlation between bands is extremely high, as shown in Fig. II-4-3-4-2, and the slope is almost constant among scenes on the same day. As conditions of the air differ on different days, the slope between adjacent bands also differs. But if this slope is made to be consistent, it will be possible to unify the intensity ratio among bands.

Among adjacent bands except Band 3/4, a scatter diagram with good concentration can be prepared, and it is possible to determine the slope from the shape and distribution of the region with this concentration. Here, using data used by the METI (2001), we examined in what areas materials very close to a straight line drawn from the scatter diagram are distributed.

For identification of materials from the scatter diagram, seven regression expressions of Bands 1/2, 2/3, and 4/5 to 8/9, were used for the scatter diagram, and pexels with radiance within the range of ± 5 were extracted from all of seven straight line expressions. This is called a high correlation region here. The Fig. II-4-3-4-3a is a false color image of BGR = 247, and areas expressed with green are regions alteration minerals are distributed.

The Fig. II-4-3-4-3b shows where changes in the color tone are emphasized by the band ratioing composite after extraction of the high correlation regions alone under the conditions mentioned above. Black regions are those that do not satisfy the conditions, and it is found that regions containing alteration minerals are completely excluded. In addition, many bare rock regions are excluded, and high correlation regions mainly consist of Pampa. In this analysis, six scenes were covered. In regions outlined under this condition, mainly Pampa in areas (where alteration minerals are not distributed in the upstream) has been mapped, and it has been clarified that the characteristics of reflectance spectra of materials in Pampa do not differ practically in any area. Therefore, it can be considered that if such materials can be mapped, the relation between bands can be converted into the fixed relation even if the analysis area is changed.

Spectra reflectance in these high correlation regions show a spectrum reflectance pattern without characteristics where reflectance increases monotonously as wavelength become long. From these mentioned above, it can be considered that outlined materials in the high correlation regions are a mixture of various rocks, and the surface is covered with oxidized minerals (Fig. II-4-3-4-4).

Extraction of high correlation regions was carried out in the following order.

① Preparing a scatter diagram between adjacent bands per scene.

② Drawing a straight line in the direction of the largest extension from the distribution shape on the scatter diagram. In this case, there is no necessity of drawing a straight line on the scatter diagram that is difficult to judge. This straight line must pass through the origin. For this purpose, the pass radiance is obtained in advance, and correction is made to the radiance value.

③ Calculating the slope of the straight line and setting a conditional expression.

④ Mapping out pixels meeting the conditions, making them images, and confirming that Pampa has been extracted.

By the work mentioned above, it is possible to identify standard materials without characteristics in spectra reflectance. The next work is to prepare again scatter diagrams between bands only in high correlation regions. Although scatter diagrams are prepared only between adjacent bands in the work done so far, scatter diagrams among all bands (36 combinations) are prepared here.

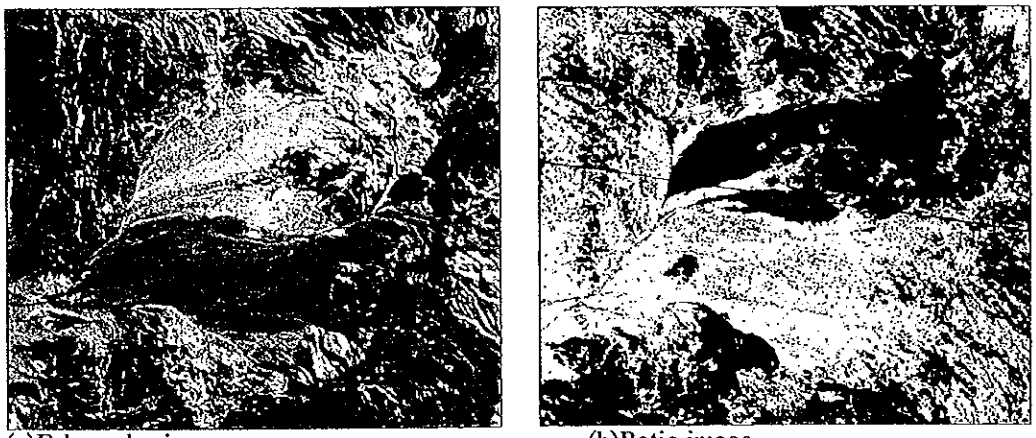

(a)False color image (b)Ratio image

Fig.II-4-3-4-3 Distribution of surface materials selected by high correlation value

Fig.II-4-3-4-4 An example of "Pampa" area selected by high correlation pixels of ASTER bands (El Salvador, Chile)

(3) Pseudo reflectance conversion

Scatter diagrams prepared only from data of high correlation regions have higher concentration and are distributed in a narrower region than scatter diagrams prepared from data of all regions. When a scatter diagram is prepared from all regions in the bands located apart, plotted data has poor concentration, and it is difficult to draw a straight line. By contrast, with data of high correlation regions, it is possible prepare a scatter diagram with relatively high concentration even if the bands are apart like Band 1/9. Therefore, regression lines of Bands 2 to 9 can be drawn with Band 1 as a basis. If regression lines have been found accurately, it is possible to make conversion into image data with the same air conditions, sensors and gains as data used by the METI(2001) by making the regression expressions of Bands 1/2 to 1/9 are consistent with regression expressions of high correlation regions of data used by the said METI (2001).

As the use of Bands 1/2 to 1/9 only is not reliable, regression straight lines with Bands 2 to 8 as a basis, respectively, were also obtained. Successive calculation from this data enables the ratio between adjacent bands to be also obtained indirectly. When the ratio between adjacent bands obtained with Bands 1 to 8 as a basis, respectively, shows an almost constant value, the regression straight lines have been obtained correctly. Table II-4-3-4 shows coefficients of regression expressions between bands with Bands 1 to 3 as a basis, respectively, which are calculated from data of high correlation regions of Data 012 to 017. Table II-4-3-5 can be prepared by indirect conversion into regression expressions between adjacent bands.

Furthermore, by the use of Bands 1/2 and 2/3, regression coefficients with Bands 2 and 3 as a basis, respectively, can be converted into those with Band 1 as a basis, as shown in Table II-4-3-6.

Regression coefficients between adjacent bands have been obtained from a scatter diagram prepared by extracting high correlation regions from data of the METI(2001), as shown in Table II-4-3-7. In a comparison between Table II-4-3-7 and Table II-4-3-6, coefficients are around 1 on Table II-4-3-6, while the luminance value in and after Band 3 is low, and coefficients of more than 2 are calculated on Table II-4-3-6. Like this, if the times of takes are different, the slope of a graph will change greatly and it is realized that the relation between bands changes greatly according to the conditions of the takes.

It is possible to change data to be data with the same conditions of obtaining as that data used by the METI (2001) by making the regression coefficients in Table II-4-3-6 consistent with those in Table II-4-3-7. Because the METI(2001) has measured the values of reflectance spectra on-site samples, pseudo reflectance conversion coefficients have been calculated. Therefore, pseudo reflectance conversion of the analysis area can be done by correcting a regression coefficient in the analysis area to be a value in Table II-4-3-7, and then multiplying a pseudo reflectance conversion coefficient.

Table II-4-3-4 Regression coefficients of band to band registration based on band 1 to 3

[Band1base]

	4/3	5/3	6/3	7/3	8/3	9/3
Dat012	0.831	0.788	0.836	0.822	0.919	0.933
Dat013	0.773	0.723	0.760	0.755	0.836	0.869
Dat014	0.731	0.720	0.793	0.749	0.857	0.886
Dat015	0.773	0.731	0.869	0.802	0.935	0.971
Dat016	0.682	0.665	0.729	0.711	0.804	0.840
Dat017	0.848	0.799	0.883	0.807	0.869	0.909
平均	0.773	0.738	0.812	0.774	0.870	0.901
std.error	**0.062**	**0.049**	**0.061**	**0.043**	**0.050**	**0.047**

[Band2base]

	4/3	5/3	6/3	7/3	8/3	9/3
Dat012	0.747	0.702	0.758	0.731	0.814	0.840
Dat013	0.711	0.689	0.731	0.705	0.796	0.820
Dat014	0.685	0.650	0.697	0.705	0.784	0.791
Dat015	0.702	0.676	0.764	0.720	0.833	0.868
Dat016	0.705	0.705	0.744	0.718	0.807	0.820
Dat017	0.747	0.758	0.810	0.770	0.851	0.880
平均	0.716	0.697	0.751	0.725	0.814	0.836
std.error	**0.025**	**0.036**	**0.038**	**0.024**	**0.025**	**0.033**

[Band3base]

	4/3	5/3	6/3	7/3	8/3	9/3
Dat012	0.959	0.890	0.950	0.939	1.072	1.095
Dat013	0.948	0.901	0.974	0.956	1.085	1.085
Dat014	0.933	0.898	0.982	0.956	1.085	1.110
Dat015	0.898	0.872	0.935	0.930	1.076	1.065
Dat016	0.959	0.942	0.989	0.968	1.110	1.120
Dat017	1.030	0.974	1.033	0.977	1.124	1.154
平均	0.954	0.913	0.977	0.954	1.092	1.105
std.error	**0.043**	**0.038**	**0.034**	**0.017**	**0.020**	**0.031**

Table II-4-3-5 Regression coefficients of band to band registration based on band 1 to 3 for neighbor bands

[Band1base]

	5/4	6/5	7/6	8/7	9/8
Dat012	0.949	1.061	0.984	1.117	1.015
Dat013	0.936	1.051	0.993	1.108	1.040
Dat014	0.985	1.101	0.944	1.143	1.034
Dat015	0.947	1.188	0.922	1.167	1.038
Dat016	0.976	1.095	0.975	1.132	1.045
Dat017	0.942	1.105	0.914	1.077	1.046
平均	0.956	1.100	0.955	1.124	1.036
std.error	0.020	0.048	0.033	0.031	0.011
adj. band ratio	0.954	1.098	0.966	1.133	1.028
absolute err	0.001	0.002	0.011	0.009	0.008

[Band2base]

	5/4	6/5	7/6	8/7	9/8
Dat012	0.941	1.078	0.965	1.113	1.032
Dat013	0.969	1.062	0.964	1.129	1.029
Dat014	0.950	1.072	1.012	1.111	1.009
Dat015	0.963	1.130	0.942	1.157	1.041
Dat016	1.000	1.055	0.965	1.125	1.015
Dat017	1.015	1.069	0.951	1.106	1.034
average	0.973	1.078	0.967	1.123	1.027
std.error	0.029	0.027	0.024	0.019	0.012
adj. band ratio	0.954	1.098	0.966	1.133	1.028
absolute err.	0.019	0.020	0.001	0.010	0.001

[Band3base]

	5/4	6/5	7/6	8/7	9/8
Dat012	0.928	1.068	0.988	1.142	1.021
Dat013	0.951	1.081	0.982	1.135	1.000
Dat014	0.963	1.094	0.973	1.135	1.023
Dat015	0.971	1.073	0.994	1.157	0.990
Dat016	0.983	1.050	0.979	1.146	1.009
Dat017	0.946	1.060	0.946	1.151	1.027
average	0.957	1.071	0.977	1.144	1.012
std.error	0.019	0.015	0.017	0.009	0.015
adj. band ratio	0.954	1.098	0.966	1.133	1.028
absolute err.	0.003	0.027	0.011	0.011	0.016

Table II-4-3-6 Regression coefficiens for band to band registration based on band1

baseBand	2/1	3/1	4/1	5/1	6/1	7/1	8/1	9/1
Band3	1.093	0.818	0.781	0.747	0.799	0.781	0.893	0.904
Band1	1.093	0.818	0.773	0.738	0.812	0.774	0.870	0.901
Band2	1.093	0.818	0.783	0.762	0.821	0.792	0.890	0.914
average	**1.093**	**0.818**	**0.779**	**0.749**	**0.811**	**0.782**	**0.884**	**0.906**

Table II-4-3-7 Regression coefficiens for band to band registration based on METI(2001)

2/1	3/1	4/1	5/1	6/1	7/1	8/1	9/1
1.318	**1.741**	**1.851**	**1.894**	**1.983**	**1.930**	**2.058**	**2.132**

4-3-5 Removing vegetation effects

Although little vegetation is recognized in Data 012 to 017, it is recognized in Data 201 to 203, Data 6200, 6201 and 6601. Plants are widely distributed, particularly in Data 6201 and 6601. In such semi-vegetation areas, it is necessary to remove the influence of reflectance spectra of plants from the radiance data of each pixel, and mineral identification must be carried out with the corrected data. For spectral reflectance spectra of materials mixed with several kinds of minerals, consideration must be given to several times of scattering and absorption on the mineral surface. Spectral reflectance spectra change nonlinearly versus the quantity ratio of minerals. By contrast, in the case where soil/bare rock and plants exist together, because soil or bare rock is sufficiently away from plants, the influence of scattering/absorption is small, and the reflectance spectra can be synthesized in a linear shape by the use of the area ratio between rock/soil and plants. In this case, strictly speaking, it is necessary to know the reflectance spectra and their quantity ratios of soil, bare rock and plants. Practically, however, as it is impossible to know such information at each point, some assumption is required.

Here, the influence of vegetation was removed on the assumption, from the fact that the SAVI (Soil Adjust Vegetation Index) functions as an index of the percentage of vegetational cover, and that one spectral reflectance spectrum can represent reflectance spectra of plants. All scenes were applied, except Data 012 to 017 where almost no vegetation is recognized. The SAVI is defined by the following expression, and the unit of value used in it is albedo (0 - 1).

SAVI = (NIR - red) /(NIR + red)*(1+L)

red: ASTER Band 2, NIR: ASTER Band 3, L: Index (0 -1, usually 0.5)

4-3-6 Processing of false color images and the band ratioing composites

(1). False color images

ASTER data consists of three VNIR bands (excluding backward-view images), six SWIR bands and five TIR bands. False color images are prepared by selecting three kinds of appropriate combination of bands from these bands according to the purpose of analysis. In this work, the following two false color images were prepared.

① BGR = 123

② BGR = 147

Those of ① are false color images with three VNIR bands used, and their characteristic is high resolution (15 m/pixel). Therefore, these images can be used as a map to replace a geological map of the field survey. Particularly in areas where the geological map is not renewed frequently, there may be roads that do not show on the geological map, and/or locations of roads may be very different from their actual locations even if they are shown on the map in some cases. On these false color images, bare rocks and deserts are expressed with a brownish color tone, which is not suitable for geological analysis such as the identification of rock.

② is a false color image made by combining one VNIR band and two SWIR bands, and is effective for geological mapping and analysis including those of alteration zones. Alteration zones are composed of alteration minerals such as quartz, sericite, alunite, kaolinite and chlorite. Among these, sericite, alunite and kaolinite show characteristic absorption in the SWIR region and show large absorption particularly in SWIR Band 7. As sericite, kaolinite and alunite generally show high reflectance in Band 5, the decrease in reflectance is remarkable from Band 5 to Band 7. Therefore, it is possible to express alteration zones in a color tone clearly different from that of the vicinity on the false color image with Bands 5 and 7 used. On this false color image, an alteration zone is expressed as slightly bluish green because the radiance value in Band 5 allotted to green is high and the luminance value in Band 7 allotted to red is low. By contrast, non-alteration rock is generally expressed in a yellowish to brownish tone because the radiance value in Band 7 allotted to red is high since there is no absorption in Band 7. When the purpose is not extraction of alteration zones but identification of rocks, the false color image of non-correlation stretches, etc. is used in some cases.

(2) Band ratioing

① Principle of band ratioing

Spectral radiance is observed on the optical sensor, and the radiance of an earth material as observed by the sensor, N_i (unit: mW/cm^2 sr), can be expressed by the following equation:

$$N_i=(1/\pi)(H_iR_iT_iA_i)+N_{pi}$$

where,

H is sunlight irradiance, R is reflectance of an earth material, T is atmospheric transmittance (vertical), A is the coefficient determined by both the angle formed by the line between the sun and the earth material and the angle formed by the earth material and the sensor, N_p is the path radiance, and i is a sensor band.

Because A becomes a constant value regardless of the channel and H and T take a value fixed by each channel, if N_p can be assumed, the spectral characteristic can be emphasized by the ratio between the two channels. This means that when looking into the ratio between the channel of the maximum value and the channel of the minimum value in the reflectance spectral pattern of a mineral, a mineral-containing pixel makes the ratio larger to make it easier to discriminate itself from a pixel of no mineral content. The basic idea of band ratioing is to apply this characteristic to the emphatic presentation of a certain mineral distribution area in images.

The band ratioing places the minimum digital value as the atmospheric path radiance, obtains the value by deducting the minimum value from the digital value of each band, and obtains the ratio between the bands of these values. The ratio between the bands (value of band ratioing) is usually in a range of 0 to 10, but density conversion is necessary to express the ratio between bands in the image, similar to the false color image. For density conversion, standard deviation and an average value of band ratioing values were calculated, and bias and gain were calculated so that the average of the band ratioing values would be 128 and 3σ would have 128 graduations of digital values.

②Band ratioing

For discriminating of alteration zones by band ratioing, band ratioing of RGB = 5/7, 5/4 and 3/1 is relatively frequently used for LANDSAT TM. With this calculation used, as alteration minerals show absorption around 2μ and 5/7 of the band ratioing value shows a large value in alteration zones, alteration zones are expressed as slightly reddish white. Because LANDSAT TM has a sensor with only one band (Band 7) around the wavelength of 2μ, alteration minerals cannot be subdivided. However, the ASTER sensor has five bands, Bands 5 to 9, around the wavelength of 2μ, and, therefore, alteration minerals can be identified more minutely from their characteristics of absorption.

In this work, two kinds of band ratioing were carried out; one is a method whose purpose is extraction of alteration zones, and the other is emphasized band ratioing where the difference of alteration minerals in alteration zones is expressed as a difference in the color tone. Both have the same combination of band ratioing, and 4/5, 4/6 and 4/7 were used as BGR.

As the object of the former was extraction of alteration zones, band ratioing values were calculated from the whole of one scene, and, after calculation of their average value and standard

deviation, gain to be used for density conversion was determined. In the latter method, band ratioing values were calculated only from data of regions extracted as alteration zones (regions where more similar rocks are distributed) and gain to be used for density conversion was determined. Therefore, the latter was given a larger gain than the former.

Calculation expressions to be used for band ratioing are 4/5, 4/6 and 4/7. When alunite, kaolinite and sericite are considered as alteration minerals, the characteristic of their reflectance spectra is that reflectance drops on the side of the longer wavelength, with that of Band 4 as the maximum value. To the contrary, reflectance of quartz, hematite and goethite, which are recognized universally on the ground surface, reaches the maximum value around Bands 4 to 5 but does not drop on the side of a longer wavelength than these. Therefore, in all of the three band ratioing calculations with Band 4 set as a numerator, an alteration zone shows a large band ratioing value because the denominators are small, while a non-alteration zone shows a small band ratioing value. Because of this, alteration zones look bright white on the band ratioing composite with multiplication by the gain calculated from the whole region, and alteration zones can be clearly distinguished and identified on the image.

It is necessary for emphasized band ratioing to extract an alteration zone and an assumed region in advance by some method. For this processing, a method called the threshold segregation method is generally used. It includes a technique where, using the band ratioing composite mentioned above, only regions that show higher values than a certain value are extracted. Here, we used a method of extracting standard materials (a region consisting of talus sediments such as Pampa and materials with almost similar characteristics of reflectance spectra) by the pseudo reflectance conversion method. This extracted standard material exists in the non-alteration zone without clear absorption characteristics. Therefore, alteration zones are contained in other areas.

On the image with density conversion where band ratioing is carried out for areas except those with standard materials, it is possible to express the difference of kinds of minerals as the difference in the color tone according to kinds of alteration minerals comprising alteration zones. For example, as reflectance spectra of alunite has the relationship of "Band 4>>Band 5<Band 6<Band 7," it is expected that alunite will look pale. Reflectance of kaolinite has the relationship of "Band 4>>Band 5 ≒ Band 6<Band 7," and it is presumed that kaolinite will show a pale color that is slightly greenish in comparison with alunite. Although reflectance spectra of sericite are somewhat similar to those of kaolinite, as the drop of reflectance in Bands 4 to 5 is small, it is presumed that sericite will have a color tone with less lightness than kaolinite. In the case of chlorite, because reflectance falls monotonously as the relation is "Band 4>Band 5>Band 6>Band 7," it is considered that chlorite presents a reddish dark color.

As mentioned above, if band ratioing is carried out targeting only regions containing alteration zones, it is possible to prepare an image where a difference of dominant kinds of

alternation minerals is expressed by a difference in the color tone. Emphasized band ratioing allows the difference of dominant kinds of minerals to be expressed by the color tone, but it does not enable presumption of the kinds of minerals. This is because a statistic is used for calculation of bias, and gain in emphasized band ratioing. If only a certain kind of alteration minerals is dominant, the above-mentioned color tones will not be shown. Namely, it can be said that only in the case where minerals other than alunite are also distributed, reflectance spectra of alunite present the above-mentioned characteristics "relatively." In addition, when alteration zones are compared among scenes, unless kinds and quantitative ratios of alteration minerals distributed in each scene are equal, minerals cannot be assumed from a difference in the color tone. Practically, it is impossible to confirm this assumption. Even if this assumption is established, since the surface layer generally comprises two or more kinds of minerals, a disadvantage of band ratioing is that it is impossible to presume kinds of minerals existing simultaneously and to know their quantitative ratios even if dominant kinds of minerals can be presumed from the difference in the color tone.

4-3-7 Identification of alteration minerals

According to the operations described in the preceding chapters, conversion into pseudo reflectance and correction of vegetation effect were carried out. Next, sensitive identification of minerals with iso-grain model was executed based on this pseudo reflectance data. Synthetic reflectance spectra were calculated by simulation by the use of a iso-grain model in this analysis. The greatest characteristic of this analysis is that it is possible to calculate reflectance spectra with any mixture ratio in the multiple componentsystem, and to relatively accurately simulate reflectance spectra of the actually measured values.

In the analysis methods employed so far, log residuals is marked, and the most dominant kind of minerals is identified from its absorption position. Only one component can be detected by this method. However, as the weathered layer surface of even alteration zones usually can contain hematite and goethite, identification with end members bears logical contraction. Furthermore, synthetic reflectance spectra with the addition of sericite of about 20% to goethite show characteristics of goethite, which is an end member, as shown by a broken line inside in Fig. II-4-3-7-1, and do not show characteristics of sericite, which is also an end member. This indicates that it is impossible to presume, from the characteristics of end members, the presence of an alteration mineral in the alteration zone containing a small amount of alteration minerals.

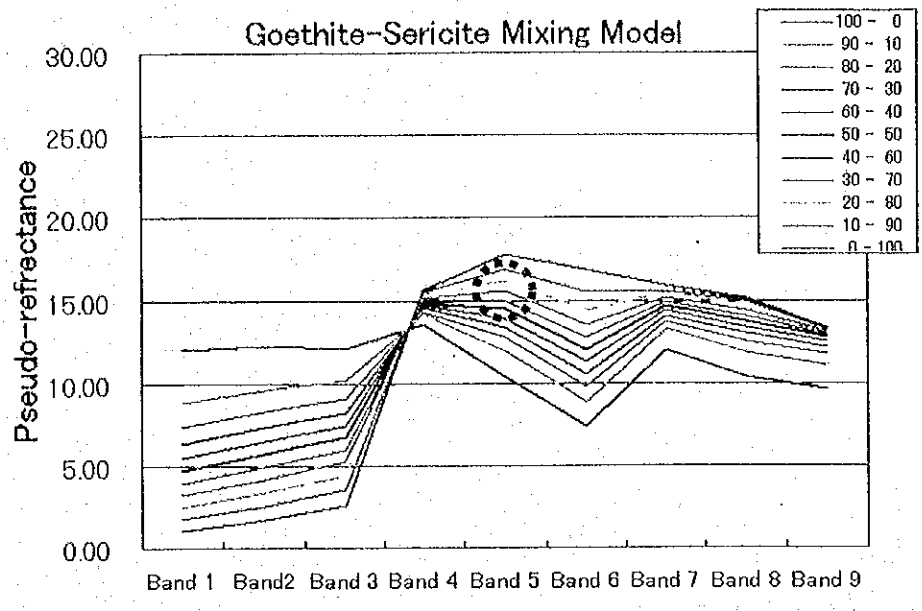

Fig.II-4-3-7-1 Spectral pattern of mixed phase of Goethite - Sericite

(1) iso-grain model

Weathered material is generally made up of two or more minerals, and the reflectance spectra of weathered materials are composed of what is summed up with reflectance spectra peculiar to the minerals comprising the material. A reflectance spectrum of each mineral and that of weathered material have a non-linear relationship. It is the "iso-grain model" that explains this relationship clearly.

For the iso-grain model, reflection from granular material is dealt with as a series of particle interactions of lights. This model unites the optical constant (the refractive index and the absorption coefficient) with two parameters (ω_1 and ω_2) that determine absorbing power and scattering power in each of the vertical and horizontal directions. Although size and shape of particles affect the accuracy of the result of calculation of the mixture ratio, modeling can be done by introducing the concept of effective particle size. For details, see the paper of the METI(2001).

Simply speaking, when surface reflectance and absorption rate per wavelength are given for each mineral, and particle size is assumed, the iso-grain model allows a synthetic spectrum to be calculated with the mixture ratio of two or more components given.

(2) Identification minerals and the database of simulation

The METI (2001) determined nine kinds of identification minerals and carried out identification using the nine components shown below:

① alunite, ② kaolinite, ③ gypsum, ④ sericite, ⑤ montmorillonite, ⑥ calcite, ⑦ chlorite, ⑧ quartz and ⑨ goethite.

As a small amount of montmorillonite was detected, and it showed somewhat large errors in matching of synthetic spectra (Even in the best matching, an average error of about 3% occurs.), montmorillonite was removed. Then, a database was prepared with the following nine components, with hematite added instead of montmorillonite. Representative alteration minerals and oxidized iron ores are shown in Fig. II-4-3-7-2.

① alunite, ② kaolinite, ③ gypsum, ④ sericite, ⑤ hematite, ⑥ calcite, ⑦ chlorite, ⑧ quartz and ⑨ goethite.

The database of mixing reflectance of minerals was prepared with multiple components in units of 10% (all mixing patterns where total percentage of minerals is 100% were considered. For example, Aln 20%, Kao 20%, Ser 30%, Goe 20% and Qtz 10%).

As mentioned above, when two kinds of alteration minerals are mixed, the shape of the reflectance spectrum changes to be non-linear to the volume ratio. Fig. II-4-3-7-3 shows the change of reflectance spectra when two kinds of alteration minerals were selected from the nine kinds and then the mixture ratio was changed in units of 10%. In this figure, the combination of minerals whose spectra change in an almost linear shape to the mixture ratio is that of sericite and kaolinite. In the case of the combinations of alunite and sericite, and kaoline and alunite, the reflectance spectra change greatly when only a small amount of sericite or kaolinite is added to alunite. When a small amount of goethite is mixed in the combination of chlorite and goethite, the reflectance spectra change greatly similarly to the case of alunite.

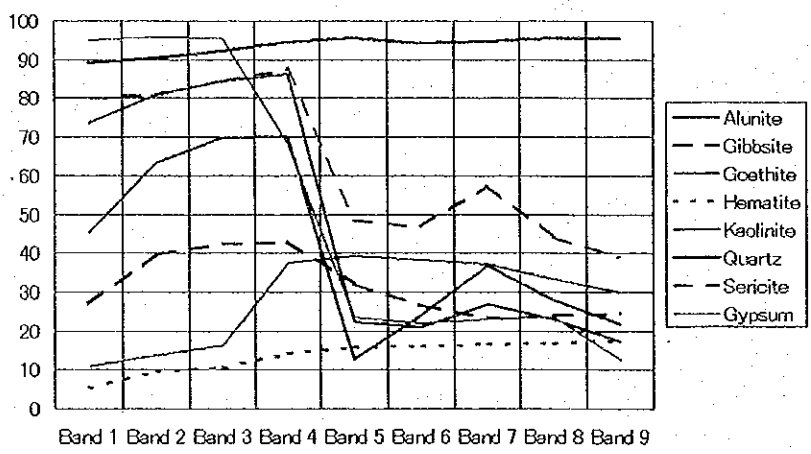

Fig.II-4-3-7-2 Spectral pattern of alteration minerals and ferro-oxide minerals in acidic alteration zone

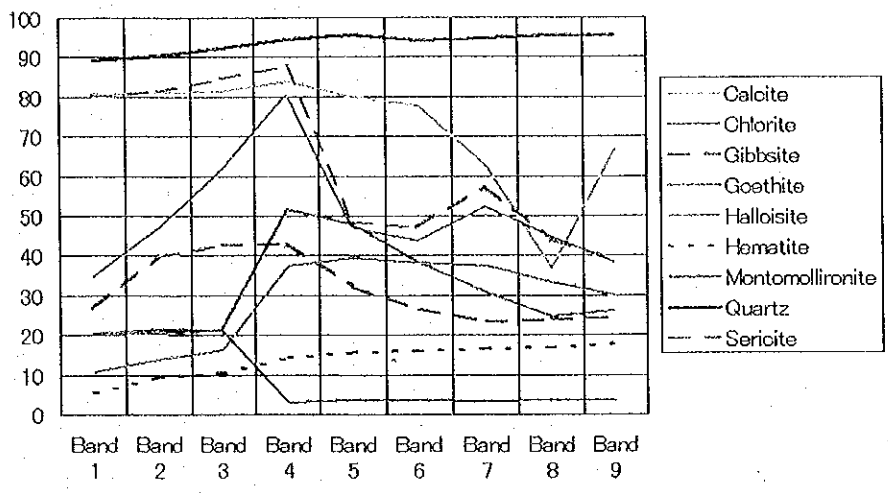

Fig.II-4-3-7-3 Spectral pattern of alteration minerals and ferro-oxide minerals in intermediate-alkali alteration zone

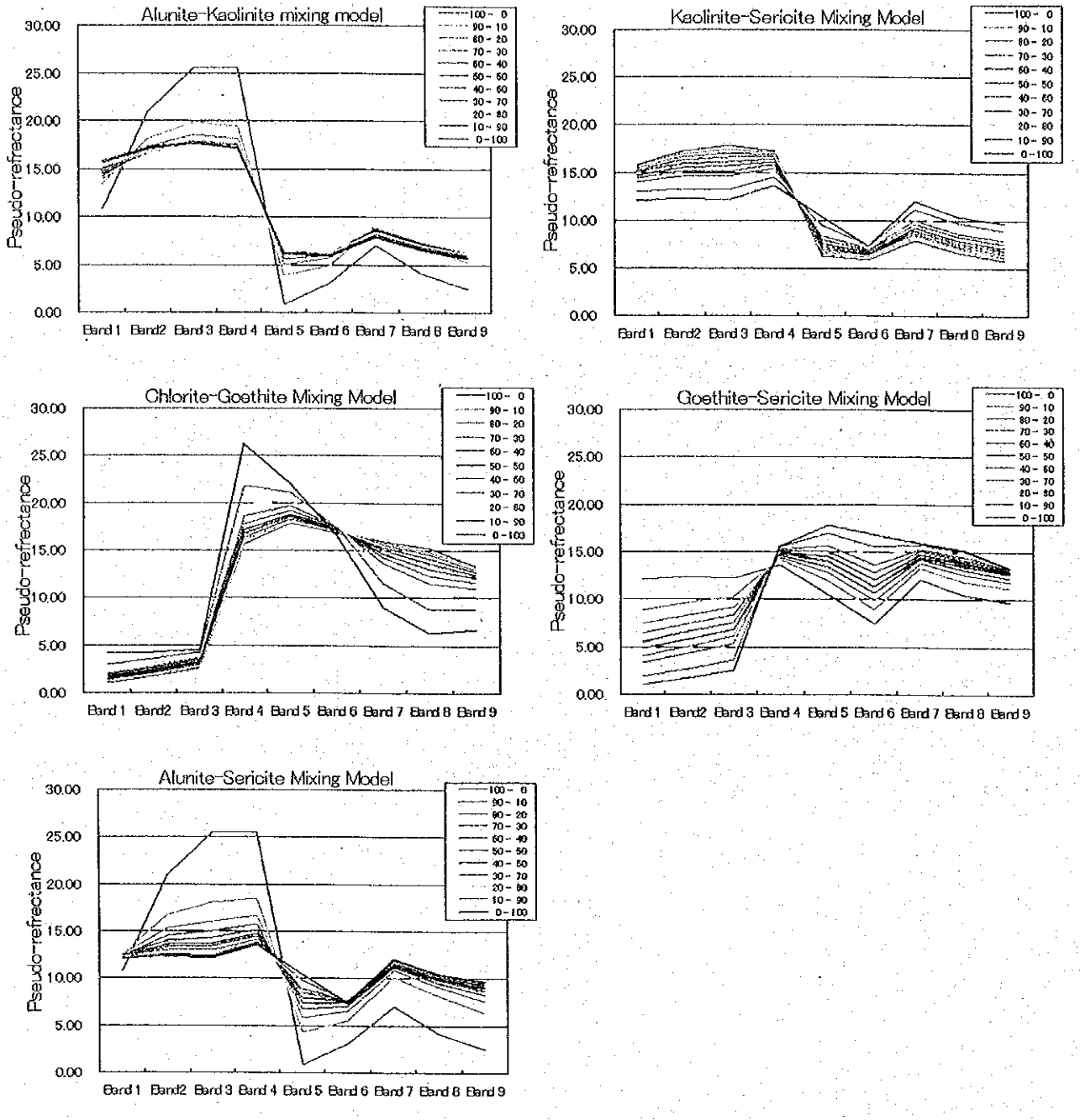

Fig.II-4-3-7-4 An example of spectral pattern mixing of two minerals

(3)Identification of minerals

A database that calculates pseudo reflectance of the combinations of minerals mixed by various volume ratios was prepared in advance, and identification of kinds of minerals was carried out by comparing this index with pseudo reflectance of each pixel. For the identification, pseudo reflectance calculated from the image is compared with pseudo reflectance of a synthetic reflectance spectrum made with the database, one by one, and the solution is a synthetic reflectance spectrum that has the smallest sum of squares of error in each band. In the actual work, the standard error from data that are the most consistent is only a little different than the standard error from the second data and the third data. Identification of minerals does not have an accuracy with which such a small difference between standard errors can be identified due to the present accuracy of conversion of pseudo reflectance, the assumption of grain of the kind of minerals and the assumption that an identification mineral is represented by one spectral reflectance. Therefore, the top three were considered as the solution, and the average value of mineral contents of the top three was determined to be the output value here. Even with this operation, it is found that the top three selections show similar mixture and composition of minerals, as shown in Table II-4-3-8.

Although an index was made with mineral mixture ratios in units of 10%, processing of one scene took one week, even though the program was made to work at high speed. Therefore, processing time was shortened (about 1/50 of the previous processing time) by the use of an index in units of 20% this time.

Table II-4-3-8 Result on the most fitted pseudo-reflectance of pixel
(top three score)

ratio of mineral composition									pseudo reflectance								
									Band1	Band2	band3	Band4	Band5	Band6	Band7	BAnd8	Band9	ERROR
Al	Cl	Ch	Ge	Gp	Hm	Ko	Qz	Sr	10.57	12.08	12.42	13.38	9.31	9.82	11.1	10.61	10.71	
40	0	0	0	0	40	20	0	0	11.11	12.29	12.59	13.20	9.48	9.69	11.27	10.51	9.87	1.09
20	0	0	0	0	40	20	20	0	10.98	12.02	12.28	12.86	9.95	9.97	11.25	10.61	10.1	1.14
20	0	0	0	20	20	0	40	0	11.09	12.55	12.92	13.54	9.46	9.85	10.96	10.67	9.53	1.21
26	**0**	**0**	**0**	**6**	**33**	**13**	**20**	**0**	← output result of identification									

First line: pseudo reflectance, Second-fourth line: composition of data base and pseudo reflectance, Fifth line: Average of above three lines, ERROR: std. error

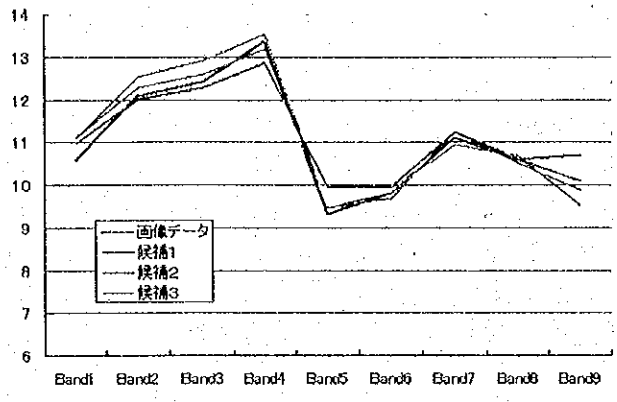

Fig.II-4-3-7-5 An example of mineral identification

(4) Results of analysis

The results of the analysis were output as contents of nine components. If one component in these output data is expressed with a concentration, a concentration distribution map can be prepared. When any three components are expressed as RBG values, a distribution diagram of three components can be prepared. Alunite and kaolinite are summed up to be dealt with as one component and are expressed as "RGB = Aln + Kao, Seo, Chl," and a distribution map of advanced argillic, phillic and porpyritic alteration zones can then be prepared. In this analysis, two components, hematite and goethite, were taken; therefore, a distribution map of iron oxide can be prepared.

In this case, the following four kinds of alteration mineral distribution maps were prepared:

① RGB = alunite, kaolinite, sericite

② RGB = alunite, goethite, sericite

③ RGB = alunite+kaolinite, sericite, chlorite

④ RGB = goethite, hematite, quartz

On the images used for this analysis, lots of clouds, shadows of clouds and salt lake sediments are distributed. In the regions of clouds, the alteration minerals are wrongly identified according to the density of clouds in some cases. In the portions of shadows, because of a very low luminance value, the influence of noise is received, and a wrong result is similarly output in some cases. As there is a distribution of rock salt, which is not included in the identification minerals, in salt lake sediments, alunite and kaolinite are identified together with gypsum. These regions identified wrongly can be identified by using the false color image together, which is troublesome work. In this analysis, interpretation of the results of analysis was made to be easily judged by digitizing, by eye, regions where clouds, their shadows and salt lake sediments were distributed and indicating them on the results of identification.

As there is a characteristic that alteration zones containing alunite and kaolinite are expressed as bright white on the band ratioing composite (BGR = 4/5, 4/6, 4/7) and as light green on the false color image (BGR = 147), alteration zones were discriminated by eye together with the results of mineral identification. In most of the regions identified as alteration zones on the band ratioing composite and the false color image, alunite, kaolinite and sericite are identified from the result of mineral identification. Therefore, it is presumed that the results of analysis are good on the whole in this stage. Alteration zones where sericite is dominant do not show clear characteristics on either the false color image or the band ratioing composite, and are generally difficult to discriminate.

Chlorite is one kind of mineral that is difficult to identify because its spectrum characteristics are unclear. If the result of this analysis of chlorite is right, it is considered, from examples of analysis so far, to be epoch-making.

Goethite and hematite were used as an oxidized iron ore in this analysis. Few distribution maps of iron oxide minerals have been prepared from satellite data so far. Furthermore, removal of vegetation information was attempted although by a simple method. Though this method makes several assumptions and has not been completed yet, if the results of identification of an alteration zone identified in vegetation of data 6201 are good, employment of this method can be expanded to data of semi-dry areas. Results of analysis of Data 6601 are shown in Fig. II-4-3-7-6 and 7.

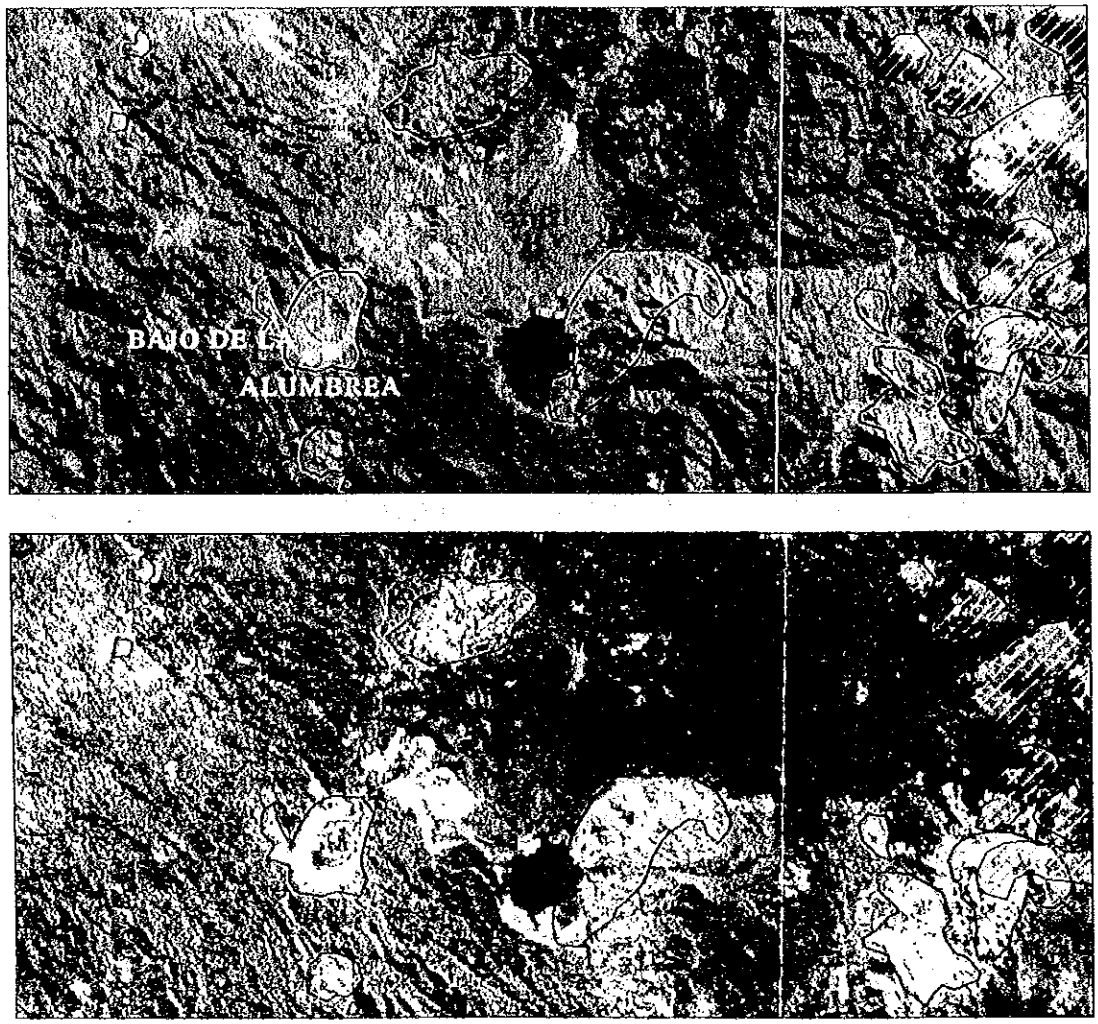

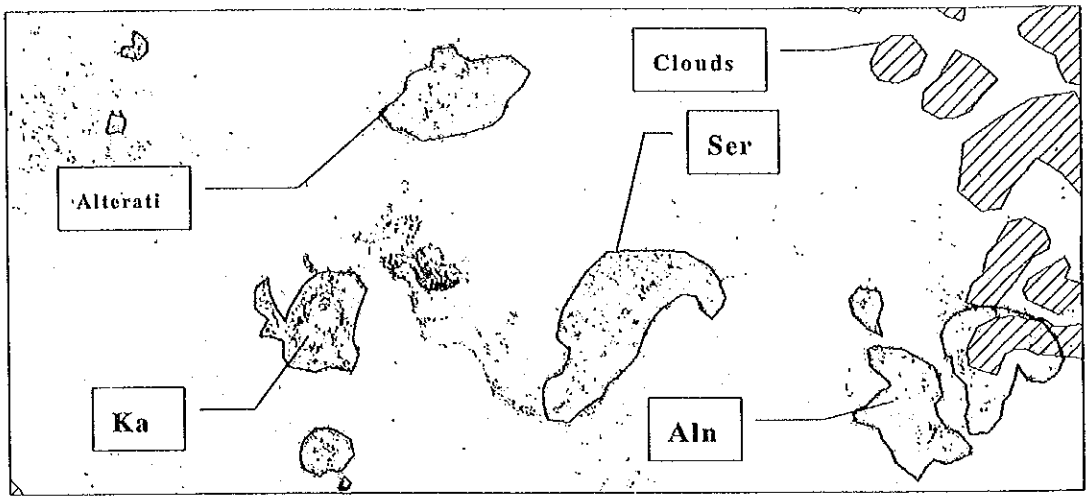

Fig.II-4-3-7-6 Mineral identification(top: BGR=247, middle: ratio image, bottom: RGB=Aln,Kao,Ser)

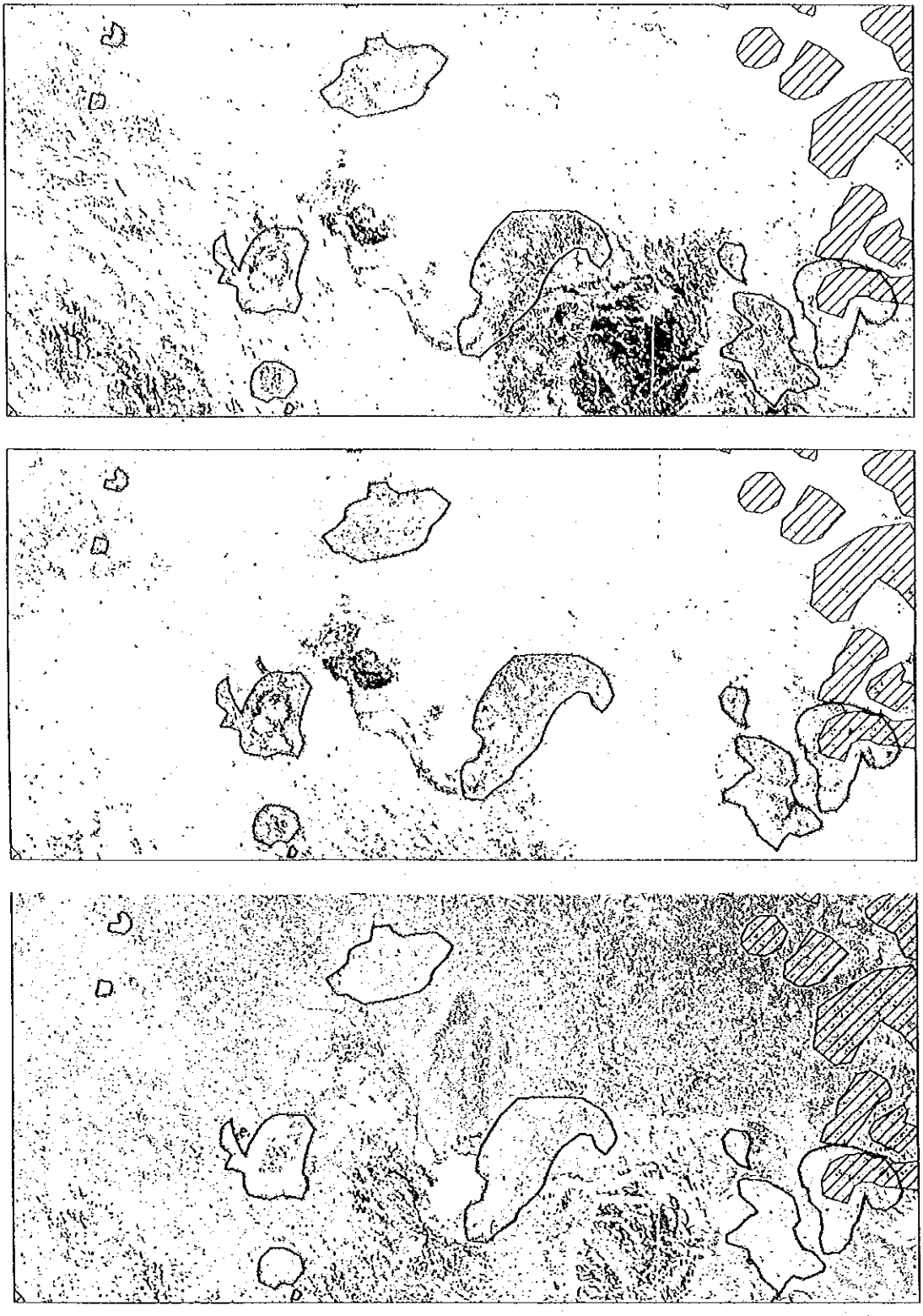

Fig.II-4-3-7-7 Mineral identification(top: RGB=Aln,Goe,Ser,
middle: RGB=Aln+Kao,Ser,Chl, bottom: RGB=Goe,Hem,Qtz)

4-3-8 SiO_2 content map

One of characteristics of the ASTER sensor is that it has five bands in the thermal infrared region. METI(1998 - 2000) and Resource and Environment Observation and Analysis Center (1991, 1992) reported examples of study to estimate SiO_2 content in igneous rock from absorption characteristics resulting from Si-O-Si vibration in the TIR of the ASTER. Particularly, the METI (2000) suggested the following SiO_2 estimation expression from four bands of the ASTER, Bands 10 to 13:

$SiO_2(\%)=56.20-271.09 \times Log((Ems[10]+Ems[11]+Ems[12])/3/Ems[13])$

Ems [n] = Emissivity of ASTER Band n

However, at the same time, the METI (2000) showed that it was necessary to re-examine the accuracy of SiO_2, including the problem of influence of desert burnish upon emissivity characteristics (Ogawa et. al., 1999), because the 95% confidence interval of the estimated volume given by the calculation expression shown above reaches as high as ± 15%.

Here, we attempted mapping of SiO_2 content in the TIR of the ASTER using the SiO_2 calculation expression mentioned above.

(1) Atmospheric correction

Radiance that is emitted from the ground surface and reaches the sensor in the thermal infrared region (8 - 13 μ m) is expressed by the following equation:

$R_\lambda = \varepsilon_\lambda B_\lambda(T)$

where λ is wavelength, ε_λ is spectral reflectance on the ground surface and T is absolute temperature on the ground surface. $B_\lambda(T)$ is radiance of a black material with temperature T and is expressed by the following equation:

$B_\lambda(T)= c_1/(\pi \lambda^5)/(\exp(c_2/\lambda T)-1)$

where:

B: Radiance of a black material [$W/m^2/st/\mu m$]

c_1: $2\pi hc^2 = 3.74 \times 10^{-16}$ Wm^2

h: Plank's constant = 6.68×10^{-34} Ws^2

c_2: $ch/k = 1.44 \times 10^4$ $\mu m^\circ K$

λ : Wavelength [μ m]

T: Temperature [° K]

c: Luminous flux = 2.99×10^8 m/s

k: Boltzmann's constant = 1.38×10^{-23} W_8 /° K

As radiance observed with a sensor includes the influence of air, radiance observed with a thermal infrared range sensor on board an airplane or satellite is expressed by the following equation (Tonooka et. al., 1997):

$R_\lambda = \{ \varepsilon_\lambda B_\lambda(T) + (1 - \varepsilon_\lambda) Rd_\lambda \} \tau_\lambda + Ru_\lambda$

where τ_λ is the spectral transmittance of air, Rd_λ is downward spectral radiance of air on the ground surface (sky brightness) and Ru_λ is upward spectral radiance from air in the optical path (optical path radiance).

For atmospheric correction, spectral radiance on the ground surface is found by removing the above-mentioned influence of air from observed radiance.

In this study, atmospheric correction parameters (τ_λ, Rd_λ and Ru_λ) in Bands 10 to 14 were found by the use of MODTRAN 3, a program for calculation of radiation transmission. While MODTRAN 3 has 6 kinds of air models and 12 kinds of aerosol models, the model of the 1976 US Standard was employed as an air model and the Desert Extinction Model was employed as an aerosol model. With consideration given to the fact that the climate of this area is dry to semi-dry, the value of vapor was determined to be that of the 1976 US Standard (average relative humidity: 19.36%).

Atmospheric correction parameters (τ_λ, Rd_λ and Ru_λ) were obtained from the following values by the use of the air model that had been established:

Air model: 1976 US Standard
Aerosol model: Desert Extinction Model
Height of the sensor: 100 km (which is the maximum value that can be set, actual height is 705 km.)
Height of ground surface: Set as 2 km
Direction of observation: Directly under (Zenith Angle = 18)
Angle of scanning in the ASTER TIR is $\pm 2.44°$, and pointing angle is $\pm 8.55°$. The difference of path length between observation with the sensor inclined most sharply and observation directly under the sensor is as small as around 2%.

Values of transmittance, sky radiance and optical path radiance in Bands 10 to 14 were weighted means, where a weight of 50% (wavelength at both ends) to 100% (central wavelength) was added to each wavelength.

(2) Temperature-emissivity separation

Regarding temperature and emissivity separation in the thermal infrared region, as the number of unknown values is larger than that of observed values, temperature and emissivity are estimated by reducing the unknown number by various methods. ASTER data (Bands 10 to 14) has five observed values, while the number of unknown values is six in total: one value of temperature and five values of emissivity.

The representative methods of estimating temperature and emissivity are described below.

* Model emissivity method

This is a method in which it is assumed that emissivity of a specific band is a fixed value throughout the target scene (Kahle, 1987).

* Normalization method

This is a method in which it is assumed that the maximum value of spectral emissivity of a pixel is constant throughout the target scene (Realmuto, 1990).

* α residual method

This is a method in which a spectrum pattern of emissivity, called an α value, is found by approximating an emission expression by the use of Wien's expression and removing the influence of temperature by taking the logarithm of the approximated emission expression (Kealy et. al., 1990).

* Band ratio method

This is a method in which a value close to the ratio of spectral emissivity is obtained by taking a radiance ratio after atmospheric correction of adjoining channels (Watson, 1992).

* Mean and max-min difference method

This is a method in which a linear relation is found between the average value and the maximum difference of emissivity of each channel, and an expression of this relation is used (Matsunaga, 1994).

In this study, temperature and emissivity were segregated by the method combining the following three methods (Gillespie et al, 1996):

* Normalized emissivity method: NEM
* Ratio method: RAT
* Mean and max-min difference method: MMD

In this calculation, emissivity on the ground surface is simply estimated by the normalized emissivity method and the ratio method. Wavelength mean emissivity is found for the scatter of the estimated values in the direction of the wavelength by the use of the empirical formula (the mean

and max-min difference method), and, using this value, the simply estimated values of emissivity on the ground surface are modified.

The flow of the calculation is described below. Input data of this calculation is upward spectral radiance on the ground surface with optical path radiance and transmittance corrected, $L_\lambda = (\varepsilon_\lambda B_\lambda(T) + (1-\varepsilon_\lambda)Rd_\lambda)$, and sky radiance Rd_λ. Output data is the temperature on the ground surface, Ts, and spectral emissivity, ε_λ.

① It is assumed that the maximum value of emissivity in Bands 10 to 14 is 0.97.

$\varepsilon_{max} = 0.97$

② Radiance with the reflecting portion on the ground surface removed from the maximum emissivity estimated and from upward spectral radiance, R_λ (referred to as "corrected radiance"), is found.

$R_\lambda' = L_\lambda - (1-\varepsilon_{max}) Rd_\lambda$

③ Temperature, T_λ, is calculated from corrected radiance in each band, R_λ', and the largest value of them shall be the estimated temperature, T.

$T_\lambda = c_2/\lambda /1n (c_1 \varepsilon_{max}/\pi R_\lambda' \lambda^5+1)$

$T = \max (T_\lambda)$

④ Black body radiance in each band at the estimated temperature is found and emissivity, ε_λ, is found by taking the ratio of the corrected radiance versus black material radiance for each band.

$\varepsilon_\lambda = R_\lambda'/B_\lambda(T)$

⑤ From this emissivity, the corrected radiance is found again according to step ②. Then, according to step ③, the estimated temperature in the band with the largest emissivity shall be the temperature on the ground surface at that point, Ts.

$R_\lambda' = L_\lambda - (1-\varepsilon_\lambda) Rd_\lambda$

$\varepsilon_{max} = \max (\varepsilon_\lambda)$

$Ts = c_2/\lambda /1n (c_1 \varepsilon_{max}/\pi R_\lambda' \lambda^5+1)$

⑥ When the mean value of black body radiance in each band, $\beta_\lambda(Ts)$, at the found temperature on the ground surface, Ts, is set as B mean, the mean value of the corrected radiance, R_λ', is set as R_{mean}, and specific emissivity, β_λ, is calculate with the following expression.

$\beta_\lambda = (R_\lambda' \times B_{mean})/\beta_\lambda(Ts) \times R'_{mean})$

⑦ When difference between the maximum value, max (β_λ), and the minimum value, min (β_λ), of specific emissivity, emissivity of each band, ε_λ, is found with the following expression.

$MMD = \max (\beta_\lambda) - \min(\beta_\lambda)$

$\varepsilon_{min} = 0.994 - 0.687 \times MMD^{0.737}$

$\varepsilon_\lambda = \beta_\lambda \times (\varepsilon_{min}/\min(\beta_\lambda))$

⑧ From the found emissivity, the temperature on the ground surface is calculated in the similar way as ⑤. Steps from ② are repeated until difference between this temperature and the temperature found previously ($\triangle Ts<0.001$).

$\varepsilon_{max} = \max(\varepsilon_{\lambda})$

$Te = c_2/\lambda / \ln(c_1 \varepsilon_{max}/\pi R_{\lambda}' \lambda^5 + 1)$

(3)Results of processing

The method described in the preceding section allows the emissivity image and the ground-surface temperature image to be prepared. The distinctive characteristic of the data used for this analysis is that scatter in the data is very large in comparison with that of the METI(2001). Especially, there are extremely small values, and, if such data is used as it is, there will be significant danger of arriving at wrong results of analysis when segregation of temperature and emissivity is calculated. Abnormally small values seem to the result of the influence of clouds. Here, the mean value and the standard deviation were calculated for each band, and those that are beyond $\pm 3\sigma$ in one or more bands of the five bands are excluded from processing.

The calculated maximum, minimum and mean values and luminance value are shown in Table II-4-3-9.

Table II-4-3-9 Emissivity value of TIR

Scene NO.		radiance					surface temperature
		band10	band11	band12	band13	band14	
Data012	min.	0.3641	0.4167	0.4476	0.5953	0.5814	264.1
	max.	1.0000	1.0000	0.9974	1.0000	1.0000	309.4
	average	0.8272	0.8194	0.7911	0.8552	0.8865	291.6
Data013	min.	0.3368	0.3574	0.3727	0.5604	0.6526	260.7
	max.	0.9999	1.0000	0.9997	1.0000	1.0000	307.7
	average	0.7728	0.7870	0.7851	0.8602	0.8838	288.7
Data014	min.	0.3496	0.3772	0.3957	0.5632	0.6372	260.2
	max.	0.9999	1.0000	0.9986	1.0000	1.0000	302.9
	average	0.7572	0.8288	0.8747	0.8986	0.8568	288.0
Dat015	min.	0.3430	0.3749	0.3804	0.5844	0.6475	259.6
	max.	0.9999	1.0000	0.9954	1.0000	1.0000	306.9
	average	0.7941	0.7921	0.7815	0.8735	0.8652	289.0

Scene NO.		radiance					surface temperature
		band10	band11	band12	band13	band14	
Data016	min.	0.3225	0.3579	0.3679	0.5525	0.6177	260.8
	max.	1.0000	1.0000	0.9992	0.9998	1.0000	311.9
	average	0.7923	0.7957	0.7779	0.8701	0.8892	293.4
Data017	min.	0.4041	0.4417	0.4640	0.6026	0.7000	268.4
	max.	0.9997	0.9998	0.9936	0.9999	1.0000	315.9
	average	0.8103	0.8138	0.8049	0.8713	0.8871	294.2
Data101	min.	0.6004	0.6097	0.5904	0.6476	0.5852	268.1
	max.	1.0000	0.9994	0.9930	0.9940	0.9925	316.2

	average	0.8677	0.8593	0.8253	0.8641	0.8703	300.2
Data102	min.	0.5832	0.5830	0.5530	0.6514	0.5973	267.9
	max.	1.0000	0.9991	0.9935	0.9928	0.9997	314.4
	average	0.8639	0.8503	0.8183	0.8621	0.8713	298.2
Data103	min.	0.5070	0.5680	0.5836	0.5031	0.3340	267.1
	max.	1.0000	1.0000	0.9999	1.0000	0.9989	312.1
	average	0.8417	0.8443	0.8276	0.8482	0.8223	293.3
Data201	min.	0.3534	0.3999	0.3992	0.6046	0.5950	249.8
	max.	0.9998	1.0000	1.0000	1.0000	0.9999	318.0
	average	0.8193	0.8066	0.7993	0.8777	0.8762	292.7
Data202	min.	0.3434	0.3853	0.3757	0.6210	0.6343	257.9
	max.	0.9990	1.0000	0.9999	1.0000	0.9995	313.7
	average	0.8209	0.8075	0.7998	0.8684	0.8874	293.5
Data203	min.	0.3160	0.3677	0.3585	0.5829	0.5710	249.0
	max.	0.9995	1.0000	0.9994	0.9998	1.0000	316.1
	average	0.8229	0.8156	0.8019	0.8717	0.8771	293.7
Data6200	min.	0.5826	0.5461	0.6787	0.7126	0.6947	276.6
	max.	0.9808	0.9990	0.9989	0.9974	0.9958	334.4
	average	0.8147	0.8725	0.8692	0.9058	0.9010	316.1
Data6201	min.	0.5356	0.5647	0.5619	0.6728	0.6502	268.1
	max.	0.9896	0.9996	0.9923	0.9983	0.9996	327.6
	average	0.8095	0.8584	0.8561	0.8943	0.8838	304.8
Data6601	min.	0.4829	0.5558	0.5679	0.6690	0.6609	268.3
	max.	0.9975	1.0000	0.9993	1.0000	0.9999	311.9
	average	0.8196	0.8331	0.8322	0.8815	0.8933	296.0
Data6602	min.	0.6013	0.6118	0.6504	0.7299	0.7324	282.9
	max.	0.9882	0.9933	0.9913	0.9991	0.9981	313.0
	average	0.7979	0.8418	0.8711	0.9075	0.8771	299.4

(4)Mapping of SiO_2 contents

A SiO_2 content map can be prepared by using emissivity data (Bands 10 to 13) and the SiO_2 conversion expression mentioned above. However, as the rock to which the conversion expression applies is silicate rock only, it is necessary to remove carbonate rock such as limestone. Fig. II-4-3-8-1 shows the SiO_2 content map and a geological map. There are still many problems in the calculation of SiO_2 content, and examination is required including that of the problem of desert burnish.

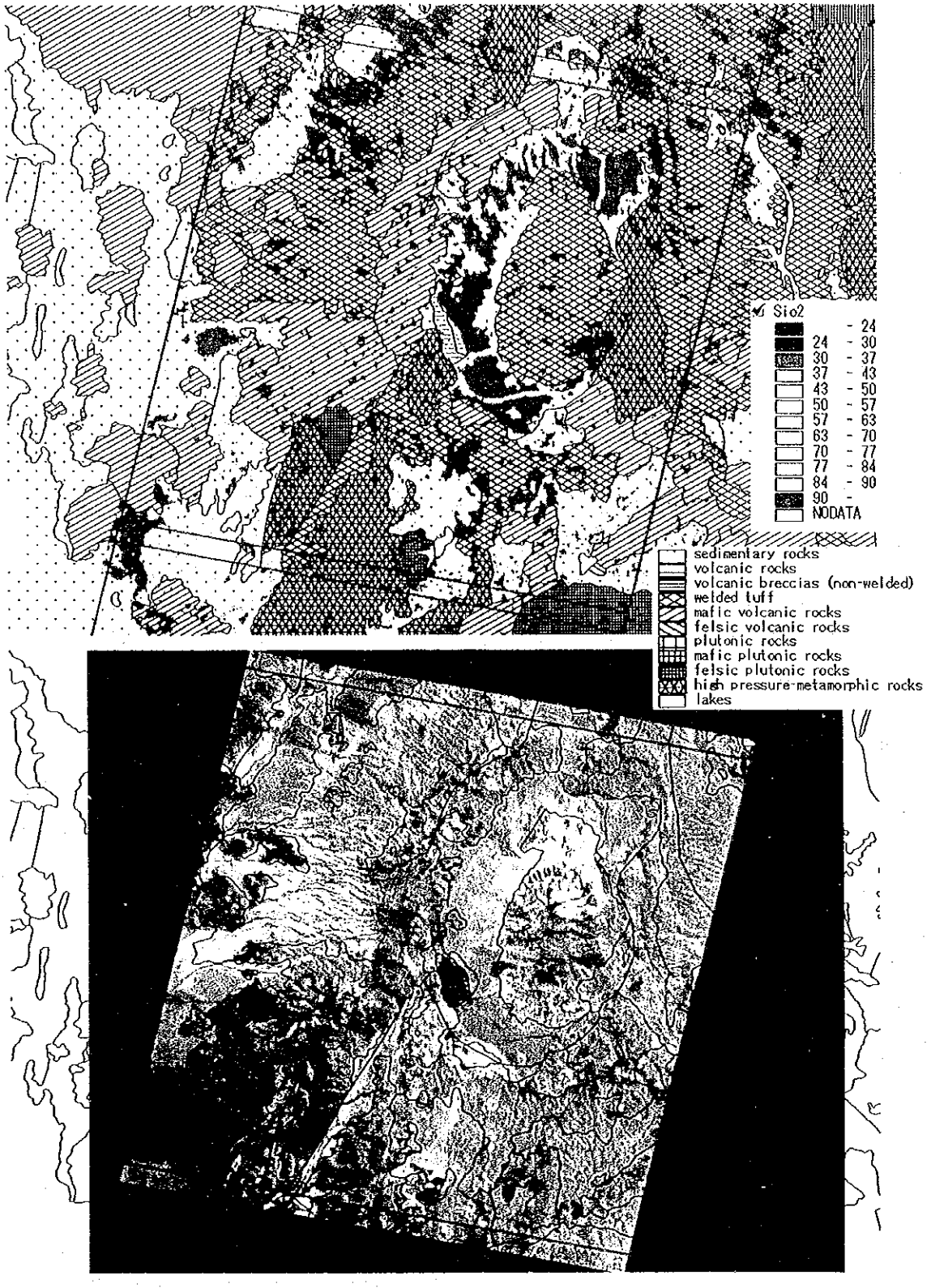

Fig.II-4-3-8-1 Comparison with SiO_2 map and geology

4-3-9 DEM(Digital Elevation Model)

(1) DEM (Digital elevation model)

Backward-looking data (VNIR 3B) obtained from the same orbit is included in ASTER data. This is image data of a backward looking from the same orbit, and can be seen in three dimensions by using the nadir looking view image (VNIR 3N) jointly. Between this pair of stereo images, there is azimuth difference (parallax) of the corresponding material on the ground surface. This difference is equivalent to a difference from the standard elevation. By measuring this azimuth difference, conversely, it is possible to find the difference from the standard elevation, i.e., elevation. Usually after taking image correlation in a nearby corresponding small region in two images, the quantity of azimuth difference is measured from the point where the correlation coefficient is the largest. Therefore, the accuracy of elevation measurement directly depends on the degree of accuracy of this image correlation. In the case of ASTER, observation time difference between two images is about 55 seconds, which is extremely short, and the ground surface at the almost same time is observed. Therefore, change of images due to optical conditions change of air condition can be restrained to be small so that image correlation with high accuracy can be expected. Applying this image correlation to the whole image obtained enables preparation of a digital elevation model (DEM) where the elevation of the round surface is measured per grid with a fixed interval.

In this work, a DEM was made from data of the three-dimensional view of five continuous scenes without clouds. Spatial resolution of the created DEM was set to be 30 m, and, at the same time, an orthographic projection conversion image with spatial resolution of 30 m was prepared for each data of the VNIR and the SWIR.

(2) Analysis with the DEM used

ASTER data has enabled make DEM relatively easily with high accuracy. Simple ways of using the DEM include a three-dimensional birds-eye view of the results of analysis. With this model, the results of analysis can be illustrated so as to be easily understood. A shadow map clarifies topographical characteristics of the survey area and is good for grasping of geology and geological structure, such as structural basins, rupture systems and volcanoes.

Such primary uses of the DEM as are mentioned above are important, but it is possible to obtain essential information that the topographical information has. For example, with the object of investigation of massive sulfide deposits in the Republic of Turkey, it is carried out to presume fault systems and pull-apart structural basins and to extract areas where wide area alteration occurs by the method of anomaly of altitudinal dispersion analysis with the ASTER DEM used (Sanga, Sato (2002): Dispersion of altitude to detect active faults and to estimate fault activities). These topographical analysis methods with the DEM used were mainly developed for geological and structural analysis of the area with vegetation, but their effect is not different for dry areas where

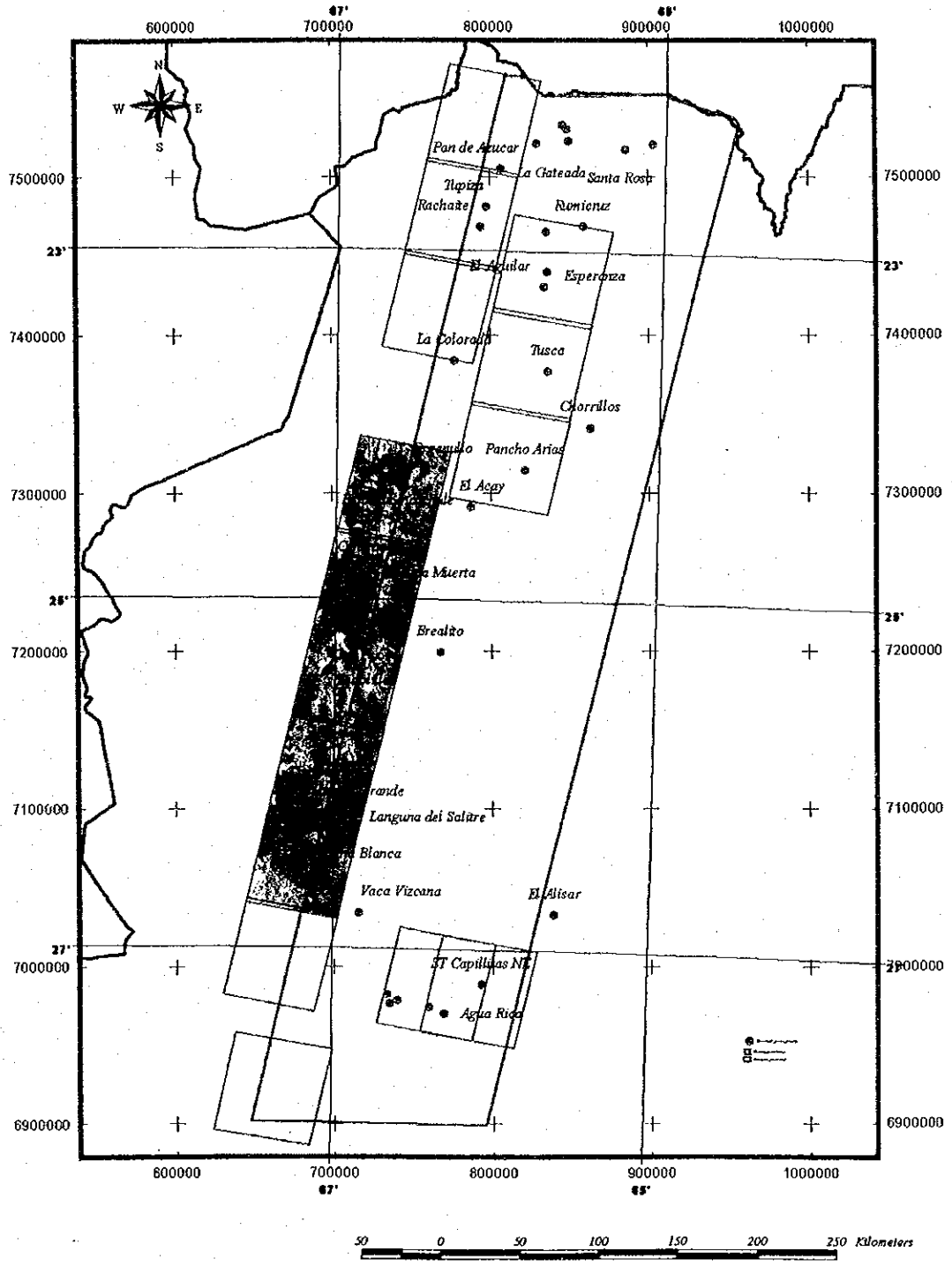

Fig.II-4-3-9-1 Index map of ASTER image area for DEM

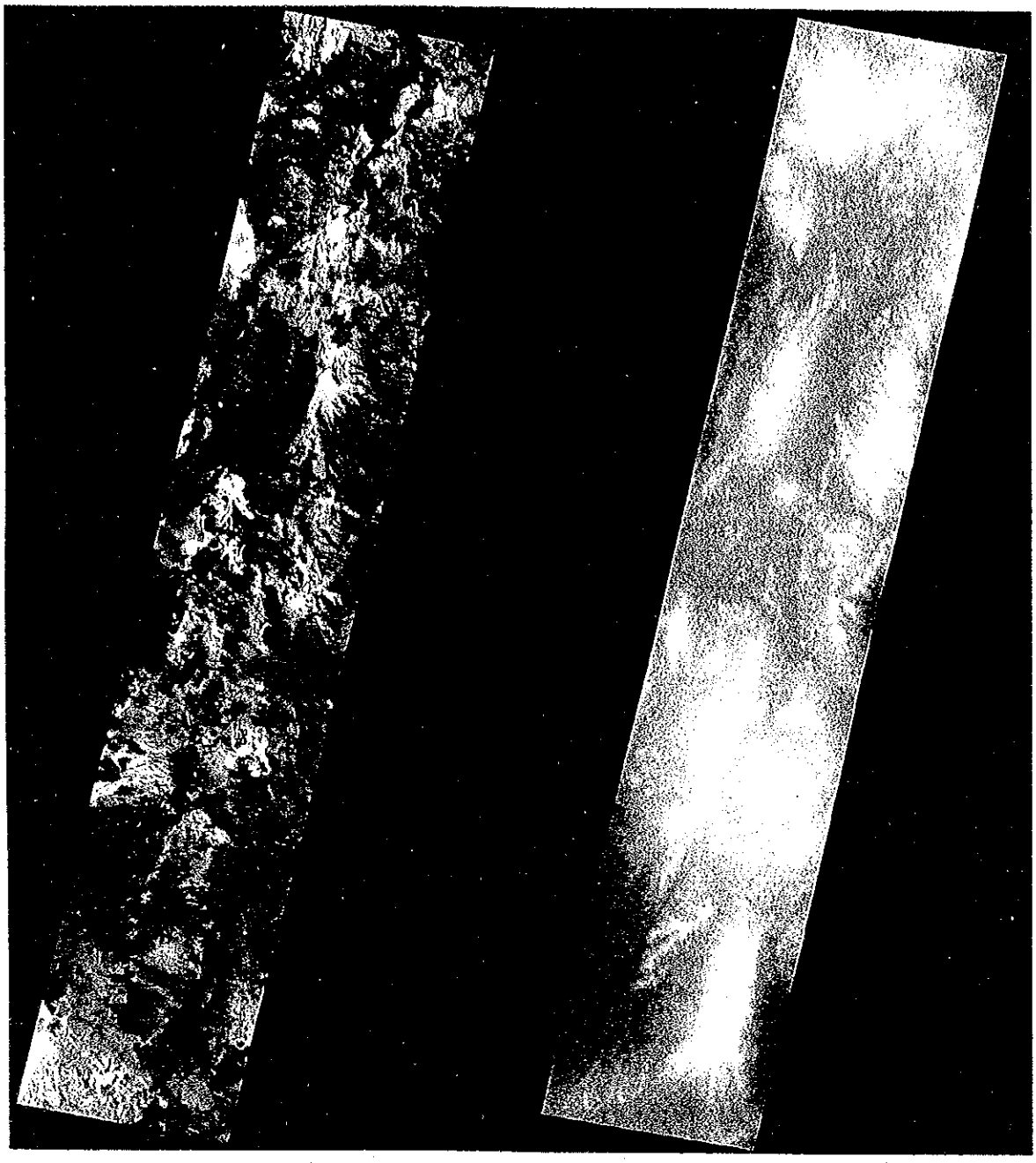

Fig.II-4-3-9-2 False color image(BGR=147) and ASTER DEM image(Sean 012-016)

bare rocks spread. For instance, if it is observed in the interpretation of the image that lithology of different ages adjoin in a linear manner, a fault structure will be presumed and the certainty is extremely high. However, in areas where similar lithology adjoin in faults, a presumption may be made after tracking continuity of topographical gaps similarly to vegetation regions. In these areas, there are cases where topographical gaps are small or where topographical gaps cannot be expressed clearly for some reason related to the sunlight direction. It is considered that methods of topographical analysis with the DEM used are also effective for these areas.

If the DEM or ASTER data where orthographic projection conversion by the DEM can be used, then higher-grade analysis with TIR data used will be possible. It is said that rocks can be identified from the false color image in the TIR by carrying out temperature and emissivity separation after atmospheric correction. There are examples where presumption of SiO_2 content from emissivity characteristics was attempted. Atmospheric correction used for these analyses, however, were analyzed on the assumption of fixed elevation, and analysis including thickness of air low layers has not been executed. Transmittance represents the decrement of radiation passing in the air, and the lower an air layer is, the larger its decrement is. This decrement varies according to wavelength, and the influence of this is larger than the difference in emissivity characteristics which change according to kinds of rocks. Therefore, if analysis is carried out with the thickness of air neglected, classification of rocks and estimation of SiO_2 content cannot be properly analyzed because the emissivity characteristics that rocks have in essence cannot be obtained properly. Regarding this problem, it is considered that, with orthogonal projection data and the DEM, accurate atmospheric correction will be able to be made from elevation data at every point.

4-3-10 Task for the future

In this analysis, reduction of vegetation was attempted with the SAVI used, and the mineral identification method could be employed for areas including those with the percentage of vegetational cover down to 30% to 40%. This method was used for only a part of the southeastern area in the survey area in this analysis, For other areas, analysis was made on the assumption of no vegetation. However, as a result of detailed observation of images, a little vegetation has been recognized in areas between mountains. Reflectance spectra in these areas with a little vegetation are composition of reflectance spectra of soil and vegetation. In the mineral identification without consideration given to vegetation, some areas were wrongly judged as alunite or kaolinite due to the influence of vegetation. Therefore, removal of vegetation before mineral identification will be indispensable work even for dry areas.

Much of the data used for this analysis was taken in winter in the survey area. Data taken in winter can be easily used for geological interpretation because height of the sun is low and topographical features are clear. On the other hand, as a south slopes of mountains are shaded, only

low luminance can be obtained and influence of noise is large, wrong judgments is made in the mineral identification in some cases. Thin clouds spread over the north part of the survey area. In such areas with thin clouds, wrong judgment were also made due to influence of clouds. The TERRA satellite works satisfactorily now and data has increased by leaps and bounds in comparison with the time of data analysis. Therefore, it is necessary to carry out re-analysis using data without clouds and obtained in summer of the survey area.

The pseudo reflectance coefficients used for this analysis were defined without acquisition of sufficient data of the field survey, and so are estimated values that lack reliability. The pseudo reflectance coefficient is a very important numerical value for the mineral identification. If this coefficient is not right, mineral identification will be also wrong. In the field verification of this fiscal year, surface reflectance was measured, and it is necessary to use pseudo reflectance coefficients corrected with data of this surface reflectance measurement.

In this analysis, two kinds of minerals, hematite and goethite, were included in identification minerals as iron oxide minerals. As one of the important iron oxide minerals for investigation of deposits is jarosite, it is necessary to add jarosite in the future analysis.